Master of Science Thesis in Electrical Engineering
Department of Electrical Engineering, Linköping University, 2023

Detection and Tracking of Elephants using Seismic Direction of Arrival Estimates

Daniel Goderik and Albin Westlund

Master of Science Thesis in Electrical Engineering

Detection and Tracking of Elephants using Seismic Direction of Arrival Estimates

Daniel Goderik and Albin Westlund

LiTH-ISY-EX–23/5590–SE

Supervisor: **Gustav Zetterqvist**
ISY, Linköping University

Examiner: **Fredrik Gustafsson**
ISY, Linköping University

Division of Automatic Control
Department of Electrical Engineering
Linköping University
SE-581 83 Linköping, Sweden

Abstract

As human settlement expands into the natural habitats of wild animals, the conflict between humans and wildlife increases. The human-elephant conflict is one that causes a tremendous amount of damage, often to poor villages close to the savannah. In this master's thesis, a system is developed, that is intended to detect, localise and track elephants from seismic vibrations generated from footsteps. The system consists of multiple devices, with three geophones, and a microprocessor each. To detect the footsteps, two different methods are evaluated. One that analyses features consistion of the normalised standard deviation, frequency peak, spectral centroid and low compared to high frequency content of a signal. These features of the signal are then compared to those of an elephant footstep. The other one compares the frequency content of the seismic wave from a footstep to an computed average of known elephant footsteps. The signal feature method performed the best with an accuracy of 89 %, and detecting 54 % of the footsteps. The detected footstep is sent to a backend where further calculations are done. With one device, estimations of the direction of arrival (DOA) angle can be made. This is done using a delay and sum algorithm. By using a Kalman filter on the DOA estimates, the bearing to the elephant can be tracked over time. From the detected elephant footsteps it has been shown that it is possible to estimate the direction of an elephant with quite high performance and by applying a Kalman filter to track the elephant, it has been shown that the filter gives better and more reasonable estimates. With two devices, a location can be estimated with triangulation and also an elephant's position can be tracked. With triangulation, where the easting position estimated to some extent, but the northing position did not give good results. By using these localisations estimates in a Kalman filter the elephant could be tracked in most of the cases with high enough performance and especially when there weren't too many high northing estimates. By using separate DOA estimations in an extended Kalman filter the easting position could be tracked fairly well, while the northing updates had some strange behaviours, most probably because of implementation error.

Acknowledgments

First and foremost, we are extremely grateful to our supervisor Gustav Zetterqvist, for all his support, and for answering all our questions regarding sensor fusion, signal processing and much more. This thesis would not have been possible without Fredrik Gustafsson, our examiner. Thank you for the opportunity to do this project, and all the adventures that has come with it. A special thanks to Carlos Vidal for all the help regarding our hardware questions, especially regarding the LILYGO. We are also grateful for the help that we got with server implementation from Martin Stenmarck from HiQ, as well as from Adam Gardell and William Hepp, which also did their master's thesis in collaboration with project Ngulia. Many thanks to the staff at Kolmården Wildlife Park, for letting us do tests there, and being helpful overall. A special thanks to Tonsak, Bua and Saonoi for being great test subjects. Thanks should also go out to Donald Bunge, Country Manager for Smart Savannahs for coming with great insight and new ideas for our thesis. We'd like to acknowledge the Department of Biology at the University of Nairobi for having us over and for the interesting discussions about our detectors. Lastly we would like to thank our friend Fred at Kenya Wildlife Service for helping us dig down our geophones and cables at Ngulia.

Linköping, June 2023
Daniel Goderik and Albin Westlund

Contents

Notation

Notations

Notation	Meaning
ϕ	Direction to source relative reference point
$y_i[k]$	Measured signal of geophone i at time k
$s[k]$	Seismic signature of an elephant footstep at time k
δ	Time for footstep
τ_i	Total delay for a footstep at geophone i
ω	Angular velocity of source relative to reference point
$D_i(\phi)$	Geometric delay to reference point from geophone i
$\hat{x}$	Triangulation estimate of the source position
p_m	Position of receiver m
μ	Mean value of a signal
σ	The standard deviation of a signal
$F[n]$	The amplitude of an FFT in bin n
$f[n]$	The frequency in bin n
f_s	Sampling frequency
C	Spectral centroid
$r_{i,ref}$	The distance a wave travels between geophone i and the reference point from direction ϕ.
c	Wave propagation speed
d	The length of each side in the equilateral triangle
r	Detection range

Abbreviations

Abbreviation	Meaning
ADC	Analog-to-Digital converter
LTE	Long Term Evolution
GPS	Global Positioning System
UDP	User Datagram Protocol
MTU	Maximum Transition Unit
PGA	Programmable Gain Amplifier
UX	User experience
GUI	Graphical User Interface
DOA	Direction of Arrival
NLS	Non-Linear Least Squares
UTM	Universal Transverse Mercator (coordinates)
FFT	Fast Fourier Transform
SIM	Subscriber Identity Module
KF	Kalman Filter
EKF	Extended Kalman Filter
CP	Constant Position
CV	Constant Velocity

1

Introduction

This master thesis is part of Project Ngulia. A collaborative project started in 2014, with multiple master's thesis projects, PhD students and other actors, that work together to develop technology that will ultimately help park rangers in Kenya preserve the wildlife on the savannah. This chapter incudes background and a formulation of the problem, as well as research question, delimitations, and a list of contributions.

1.1 Background

In many parts of the world, the human-wildlife conflict poses a great problem for both humans and wildlife. As human settlement expands, it expands into the natural habitats of wild animals. This causes the human-wildlife conflict to grow more and more abundant. In particular, elephants have been shown to cause more damage to humans than any other herbivore species [7]. Elephants can cause a tremendous amount of damage to villages struck with poverty by damaging infrastructure, and by consuming farmers crops, or even kill people. This inevitably causes irritation from humans towards the elephants and often leads to killing of the elephants, in lack of better methods. This is one of the biggest issues in elephant conservation today [25].

Traditional methods for deterring elephants, like electric fences, have been shown to be expensive to build, have big upkeep costs and, in general, being fairly unreliable [23]. There is a need for a modern, inexpensive and reliable method of keeping track of elephants near human habitats to mitigate the human-elephant conflict.

All animals make a different seismic impact when taking a step. Knowing this,

it would be possible to differentiate an elephant's footstep to other animals. By measuring seismic signals from the ground with geophones, an elephant footstep can be detected from distances where park rangers will be able to deal with the elephants before they reach the villages [29]. In this thesis, devices consisting of three geophones each will be constructed. The geophones measure seismic signals from the ground to detect, localise and track elephants.

The work in this thesis is based on the previous master's thesis by Philip Sjövik and Erik Wahledow [24]. In that thesis, a device with three geophones was built, capable of detecting elephant footsteps and calculating the direction of the elephant using a direction of arrival (DOA) algorithm. That thesis showed a promising result, and with further development, it could be quite useful in the human-elephant conflict.

1.2 Goal

The goal of this master's thesis is to build a system which detects, localises and tracks elephants from as far away as possible. The system should only indicate a detection if there is an elephant, and in no other cases. This will be achieved by measuring seismic signals from the ground. The system should be energy efficient, cheap and robust since the goal is to build a system that can be reproducible and located in distant lands.

1.3 Research questions

The report aims to answer the following research questions:

1. How well can an elephant footstep be differentiated from other animals?
2. How well can the direction of a target be estimated and tracked using a geophone array?
3. How well can an elephant be localised and tracked using two geophone arrays?

1.4 Delimitations

In this master's thesis, the developed tracking algorithm will be able to differentiate separate elephants, given that they are far enough away from each other. The method will however not be able to differentiate separate individuals in a tightly packed herd. This will be interpreted as a single individual in the tracking. There are also some hardware delimitations, one being the amount of data.

Another delimitation is power consumption. The system will be powered by solar panels and batteries, and should therefore strive for a minimal power consumption.

A majority of the data collected is from Kolmården Wildlife Park. At Kolmården, there are only Asian elephants, which is not the intended species for the final product. There are other limitations in the availability of animals at Kolmården, and many of the interesting animals of the Kenyan savannah are not available. Although some data was collected in Kenya, the majority had to be collected at Kolmården.

1.5 Contributions

As previously stated, this thesis expands on a previous thesis. However, there are many differences and contributions from this thesis. One in that the detection algorithm has completely changed. It has also been tested for false alarms from different animals to a higher extent than last year. The DOA calculations have been changed slightly as well, and tracking of the angles has been added, including multiple target tracking. Localisation is a completely new addition to the thesis as well. It uses multiple devices to triangulate the targets, which has not been done before.

1.6 Report overview

In this section, an overview of the entire report and its chapters are presented. Chapter 2 brings up some background theory to lay a foundation for the rest of the report, as well as discussing some previous related work. In Chapter 3, the system used for data collection and processing is described. Later in Chapter 4, Chapter 5, and Chapter 6, method, result and a discussion is included for the detection, DOA and tracking respectively. Chapter 7 concludes the report, summarising the key points of this thesis and answering the research questions, as well as discusses future work.

2

Theory

This chapter aims to lay a theoretical background, for better understanding of the contents of the report. The chapter includes theory about seismic waves, elephant behaviour and characteristics, as well as some previous work regarding footstep detection.

2.1 Seismic Waves

There are different kinds of seismic waves that can propagate from a source. The two main types of waves are *body waves*, and *surface waves*. Body waves, often divided into P-waves and S-waves, are able to propagate deep into the earth, whereas surface waves can not penetrate the ground very deeply. For this project, surface waves are the most relevant, and are the ones that can be detected by the geophones [17].

Based on previous research, elephant footsteps usually mostly consist of Rayleigh waves [18]. These waves rarely exceed 200 Hz, and therefore a sampling frequency of at least 400 Hz should be used when measuring elephant footsteps to avoid aliasing [9].

2.1.1 Wave propagation speed

The wave propagation speed varies to some extent, depending on the ground. For loose clay or sand, the speed is usually about 80-220 m/s [4]. This will have to be calculated for different locations, as it will be necessary for the DOA estimates.

2.2 Elephant

The elephant is the main focus of this report, and therefore it is important to know some background information about the animal. Both the footsteps of the elephant, and its lifestyle will be investigated.

2.2.1 Elephant's lifestyle

An Elephant's life is full of eating and drinking due to its enormous size. An African elephant is typically between 3–5 meters long and weighs around 2500-7000 kg [6]. An elephant spends approximately 18 hours per day eating. During a day, an elephant eats approximately 150 kg of food and drinks a large amount of water. This means that an elephant can hike up to 30 miles a day to get enough food. When elephants find food do they often stay at the same spot for hours and when they get hungry again they are going to start searching for more food [10].

Elephants also live in herds, which can be between 8–100 individuals. The herd is led by a matriarch, which is the eldest female, because of her experience and knowledge through life. The herd will follow the matriarch in the search of water, food, safe spaces and protection [1].

Elephants do not sleep much and usually only sleep two hours per day if they are in the wild. When an elephant is sleeping, another elephant is often awake to protect and keep the sleeping elephant safe. A reason for the fact that elephants sleep so little is that they eat very much and doesn't have time for sleeping too long, and also their digestion is not as effective when they are sleeping [2].

During data collection at Kolmården, relevant observations have been made about elephants habits. These elephants are enclosed and have been trained and can not be directly compared to wild elephants on the savannah. Although, when the elephants were released outside, the first instinct of the elephant was to look for food. Secondly, the elephants liked to explore the environment and when they found something interesting they stay still on the spot. For the data collection, this meant that the elephant typically would move for less than a minute, and then stand still for a longer period of time.

All these facts and observations affect the system in different ways and will be discussed further in the design of the methods used.

2.2.2 Elephant footsteps

Previous studies have been done on the characteristics of elephant footsteps and elephant footstep detection. This project is based on the work of [24]. From their measurements, an elephant footstep was shown to have most of the frequency content between 10-20 Hz. In [29], a method for detecting elephant footsteps, by analysing the signal's frequency properties. In their data collection, the elephant

footsteps had a peak at around 25 Hz, with most of the signal energy under 40 Hz. This will have to be investigated for the detection algorithm.

2.3 Footstep detection

Footstep detection using geophones is nothing new, and has been done many times before. However, it has mostly been done to detect human footstep for intruder detection and for military purposes. In [3], an algorithm that detects human footsteps is developed. Their method uses kurtosis to detect footsteps, and cadence, that is the time between footsteps, to determine if it is a human. In [21], kurtosis is also used for footstep detection, and this seems to be a popular approach, although this can not differentiate between different animals. To be able to differentiate between different animals, one would need to look at signal properties. This is done in [20], where many different features are utilised, including standard deviation, entropy, peak values, partial signal before and after the maximum peak, spectrum centroid, locations and amplitudes of peaks and power spectrum density.

3

System overview

To be able to perform triangulation, multiple geophone arrays are needed. Each geophone array consists of different hardware components which collect, convert and send data in a suitable format to the backend. This section describes each hardware component and their function. Figure 3.1 gives an overview of the entire system and its subsystems. Figure 3.2 shows a picture of the actual hardware used.

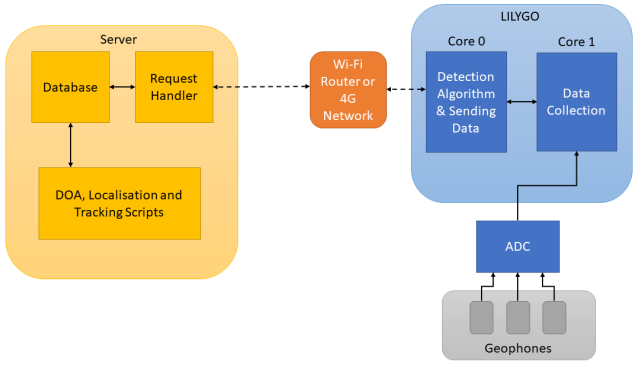

Figure 3.1: *An overview of the system and its subsystems. This can be scaled up with more LILYGOs.*

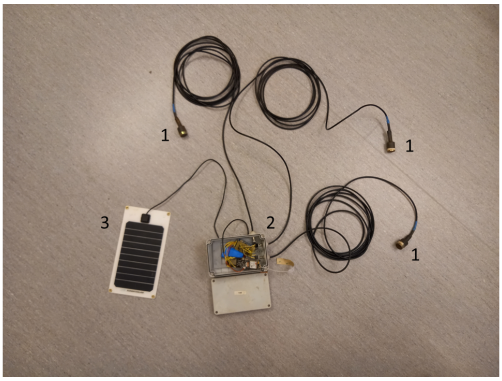

Figure 3.2: *A picture of the hardware developed in this thesis. 1) indicates the three geophones. 2) is the box that contains the microprocessor, ADC, battery, GNSS antenna and LTE antenna. 3) is the solar panel.*

3.1 Microcontroller

The microcontroller used is a LILYGO® TTGO T-SIM7000G ESP32 board. It is based on a ESP32 with an added T-SIM7000G module. The microcontroller is used to run the detection software and send data to the backend. The board features LTE for wireless communication, which allows for transition of geophone data to the backend, but can also use Wi-Fi to transfer the data. It also allows charging from solar panels and comes with a GPS antenna for localisation [28].

3.2 Analog-to-Digital Converter

The system uses the analog-to-digital converter ADS1256. It is a low noise ADC with 24-bit resolution. It also has a programmable gain amplifier (PGA) that can be programmed with a gain from 1 to 64 if needed [26]. The 24-bit resolution will hopefully allow for better data than if the 12-bit resolution ADCs, built in the ESP32, were to be used [8]. In this project, the PGA was set to 32. Figure 3.3 shows the connection between the ADC and the microcontroller.

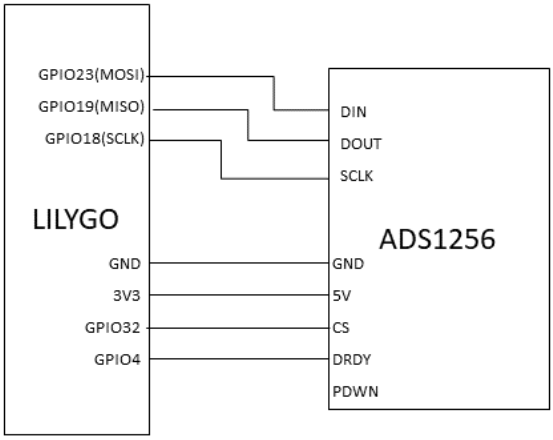

Figure 3.3: *The circuit that connects the microcontroller and the ADC.*

The ADC controls the sampling frequency. It is set to 2000 samples per second over three channels, which should result in approximately 667 on each channel. However, in reality, other processes are run that reduce the sample rate. Therefore, the set sample rate of 2000 samples per second results in a sample rate of about 474 samples per second. This is enough for the intended purpose.

3.3 Geophones

The geophone converts ground movement to voltage. The geophone used in this project is of the model *SM-24 Geophone element* [22]. For every geophone array, there is a need for three geophones to triangulate a target.

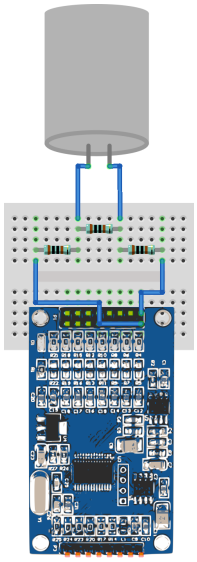

Figure 3.4: *A sketch of the circuit between the ADC and the geophones.*

Between the geophone and the ADC is a termination circuit, displayed in Figure 3.4. The 1 kΩ parallel resistor connected in between the geophone pins is used for calibration of the geophone according to the data sheet [22]. The two 1 kΩ resistors, connected in series to the ADC, are there to protect the ADC from current spikes, that could break the converter. When a vibration from the ground reaches the geophone, it is translated into a current. This current then travels through the termination circuit, and then through coaxial cables to the ADC.

3.4 Energy consumption

The system will be run on solar power. It is therefore essential to keep the power consumption to a minimum. The most power consuming component of the hardware is the LILYGO. While working under normal conditions, it draws about 200 mA [28].

The ADS1256 also has a power consumption, but much smaller. During normal settings it draws less than 10 mA [26], but if PGA is used, this could be increased with a couple of mA, but not enough to make a noticeable difference. The total draw current that can be expected from the whole system should be around 200 mA. With a supply voltage of 3.7 V, this would need a 0.74 W output from a solar panel to keep the system running during the day. However, a powerbank is needed to keep it alive at night and additional power is needed to charge this. The solar panels used have a maximum output of 6 W. The devices are equipped

with a battery pack with nominal capacity of about 6.7 Ah or 24.6 Wh.

3.5 Backend

When a detection is made by the microcontroller, the segment containing the footstep is sent to a server. From here, calculations can be made for the DOA and localisation of the elephants, as well as tracking. In the future, the data calculated in the backend can be sent to the park rangers, to aid them in their conservation work.

4

Elephant Footstep Detection

The footstep of an elephant has unique characteristics. This can be used to differentiate elephant footsteps from other animals, and detect the elephants. This chapter describes the methodology for two different detection algorithms, one based on unique signal features that the elephant footstep has, and one that compares the signal to an average elephant footstep in the frequency domain. Both methods are evaluated and compared.

4.1 Footstep extraction

Both methods need extracted segments of data, containing potential elephant footsteps. It is important that the segments are of appropriate size and to save processor power, it is advantageous that the calculations are not performed on noise, only on potential footsteps.

4.1.1 Segmentation

An elephant footstep has shown to be around 100-250 ms [19]. If a whole footstep is to be recorded, it is important that the used segments are around this length. For the real time application, a segment, or window, of at about 270 ms is used. This window corresponds to 128 samples. When a new measurement is acquired, it replaces the oldest measurement in the window buffer. This gives a sliding window of 128 samples for the real time application. If a step has been detected, the system will wait until the buffer does not have any old sample left from the last detection before testing the next segment. This is done to prevent having data from an old step and causing detection of the same step twice. Detecting the same step multiple times can cause worse quality data segments to be sent to the direction of arrival estimates.

4.1.2 Event detection

To determine if a segment includes an elephant footstep, the algorithm first detects if there is an event. This could be any type of signal that is not ambient noise. This is done by calculating the kurtosis of the segment according to Equation (4.1)

$$\text{kurtosis} = \frac{\frac{\sum_{k=1}^{N}(y[k]-\mu)^4}{N-1}}{\left(\frac{\sum_{k=1}^{N}(y[k]-\mu)^2}{N-1}\right)^2} \tag{4.1}$$

Where N is the number of samples in the window, $y[k]$ is the amplitude of sample k, and μ is the mean calculated in Equation (4.2) [14].

$$\mu = \frac{\sum_{k=1}^{N} y[k]}{N} \tag{4.2}$$

The kurtosis is a comparison of the distribution of the signal, compared to a Gaussian distribution with the same standard deviation. This means that if a signal differs from Gaussian noise, it will have a steeper peak around the mean than the noise. Therefore, kurtosis is a good measurement to differentiate an event from ambient noise. Gaussian noise usually has a kurtosis of around 3.

Two thresholds are used for the extraction of events, one higher, and one lower. If the higher threshold is met, the segment is chosen to begin 28 samples before the low threshold was first met. In Figure 4.1 the event detection is illustrated.

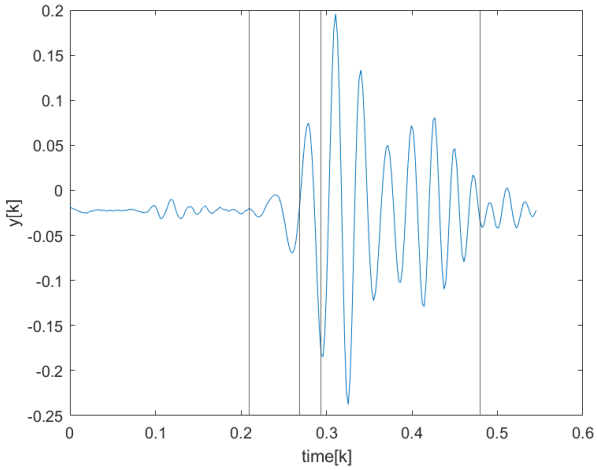

Figure 4.1: *Event detection illustrated on a seismic wave of an elephant footstep. The left and rightmost lines are the bounds of the segment. The second line to the left is the low kurtosis threshold, and third to the left is the high threshold.*

4.2 Signal features method

The signal features method uses unique characteristics of the elephant footstep to make a detection algorithm. First it does some processing of the signal, and then it compares the signal to an elephant footstep, with regard to standard deviation, frequency peak, spectral centroid and frequency distribution. Figure 4.2 gives an overview of the different parts of the signal features detection algorithm. Although hard to quantify, the reasoning behind the feature order has been chosen so that the feature that discards the most false detections is calculated first. This is done to avoid doing unnecessary calculations.

4.2.1 Filtering

An elephant's footstep has a frequency range that rarely exceeds 30 Hz [19]. To isolate the interesting part of the signal, and reduce the influence of noise when analysing the characteristics of the signal, a filter is needed. A band-pass Butterworth filter, with cutoff frequencies 4 and 45 Hz, and order 6 is used. The reason for a band-pass filter, rather than a low-pass filter, is because low frequency noise was apparent during testing. The 4 Hz cut-off frequency reduces this noise.

4.2.2 Normalisation

Before extracting characteristics of the signal, the signal is normalised. This is done in regard to the power of the segment. This means that the total power of

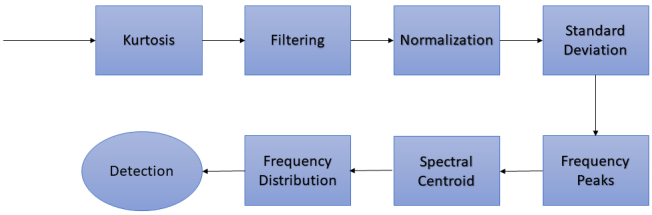

Figure 4.2: *A schematic overview of the different stages of the signal feature detection algorithm.*

the segment will equal to one after the normalisation. This will help mitigate the effects of the potential distance differences of different signals.

4.2.3 Signal features

To determine if an event is an elephant, different features are analysed and compared to those of an elephant. This section describes these signal features. For a detection to occur on a device, the criteria for the signal features must be met on all three geophones. A signal must pass all the feature tests to be classified as a footstep. The choice of parameters will be presented in Section 4.4.

Standard deviation

The first feature that is analysed is the standard deviation of the normalised signal, in the time domain. This is done in Equation (4.3).

$$\sigma^2 = \frac{1}{N}\sum_{k=1}^{N}(y[k]-\mu)^2 \tag{4.3}$$

The standard deviation will differ between different signals in the time domain, and can be used to differentiate between different signals. If the standard deviation is between a low and a high threshold, it passes the test, otherwise it is discarded.

Frequency peak

The next characteristic of the signal that will be used is its major frequency peak. To get the frequency content, a fast Fourier transform (FFT) is performed on the

signal. Next, the frequency with the highest magnitude is calculated. If the main frequency peak is in between two threshold values, it passes the test, otherwise it is discarded.

Spectral centroid

The spectral centroid uses the same FFT as for the frequency peak, and is used to determine what frequency the spectrum of the signal is centred around. It is a weighted mean of the frequency content of the signal. The calculation of the centroid is done using

$$C = \frac{\sum_{n=1}^{\frac{N}{2}+1} f[n]|F[n]|}{\sum_{n=1}^{\frac{N}{2}+1} |F[n]|}$$

where C is the centroid, N is the number of samples, $F[n]$ is the amplitude corresponding to bin n and $f[n] = \frac{nf_s}{N}$ is the frequency corresponding to bin n [16]. If the centroid is within chosen thresholds, it passes the test.

Frequency distribution

Lastly, the energy of the high frequencies is compared to the low frequency energy. This is done by filtering out the high frequencies using a 6th order Butterworth high-pass filter, with cut off-frequency 55 Hz. The energy of the low frequencies extracted from the filtered segment, described in Section 4.2.1, is divided by the energy of the high frequencies to get a ratio. If the ratio is above a certain threshold, the test is passed. This ratio can not be too low, since high frequency noise could make the detection algorithm fail. However, footsteps generally have much more energy than noise, so this should not cause a problem. Looking at the ratio between low and high frequencies is useful for two main reasons. Firstly, it filters out many animals, other than elephants, quite efficiently. Secondly, if an elephant is detected, but the segmentation is poor and the segment mostly includes ambient noise and a small part of the elephant footstep, the segment will generally have higher energy at higher frequencies than usual. These segments are not good for the direction estimation later on, so discarding them early on is a good thing.

4.3 Average footstep method

Another method for detection and characterisation, is to compare the signal to an average footstep. The interesting frequencies of the average footstep is below 45 Hz. In many datasets, a disturbance at 50 Hz was also present, therefore the average footstep is of band-pass filtered footsteps. They are filtered using a 4th order Butterworth filter with cut-off frequencies 4 Hz and 45 Hz. The signal is then normalised in regard to power. The average frequency content is then calculated by taking the average amplitude value of every frequency bin of the

FFT, over many known elephant footsteps. This yields an average normalised filtered footstep. A signal is then compared to the average signal by calculating the error of every frequency bin. If a frequency bin error is too large, the signal is discarded. If all errors are within a chosen threshold from the mean, the signal is determined as an elephant. The test has to pass on all three geophones to be deemed an elephant.

4.4 Results

In this section, the detection algorithm is evaluated. First, different animal footsteps are analysed to calculate parameters for the two algorithms. Secondly, the performance of the results of the algorithms' performances are presented.

4.4.1 Animal footstep analysis

Measurements of animal footsteps were done, both at Kolmården Wildlife Park and in Kenya. The footsteps were counted from video footage of the animals. Below, data from both locations is presented.

Kolmården Wildlife Park

The data collected is from animals at Kolmården Wildlife Park. The park has three Asian elephants (*Elephas Maximus*), one male and two females. For comparison, data was also collected from a rhino, kulans and Asian camels.

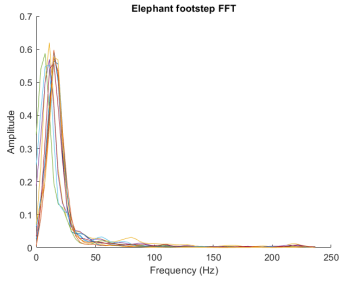

(a) *FFT of ten elephant footsteps, using a Hamming window.*

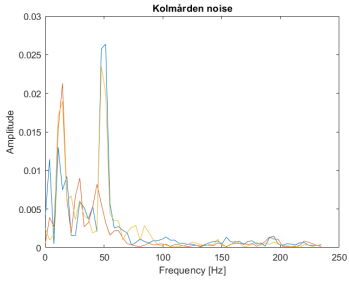

(b) *FFT of the noise at Kolmården.*

Figure 4.3a shows the FFTs of ten elephant footsteps, from a male elephant. One can see a great concentration of the frequency content between 5-30 Hz. Figure 4.3b shows the ambient noise at Kolmården, and a peak at 14 Hz and one at 50 Hz can be seen at fairly low amplitudes.

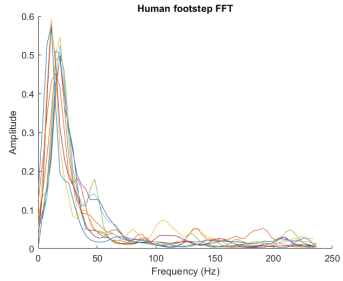

(c) FFT of 10 human footsteps, with a Hamming window.

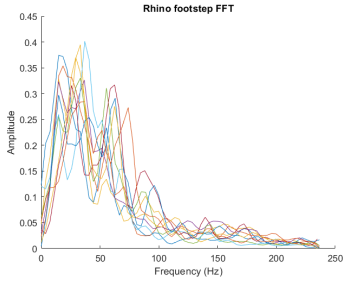

(d) FFT of 10 rhinoceros footsteps, with a Hamming window.

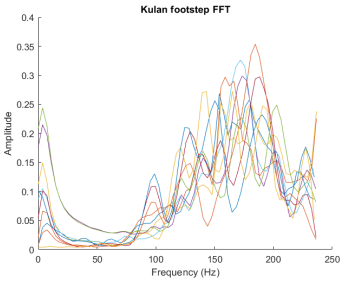

(e) FFT of 10 kulan footsteps, with a Hamming window.

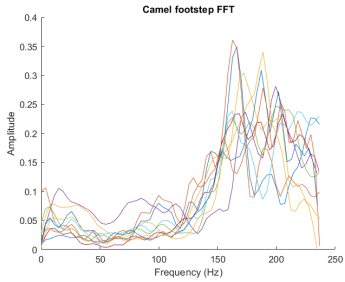

(f) FFT of 10 camel footsteps, with a Hamming window.

Figure 4.3: *FFT from 10 human, rhinoceros, kulan and camel footsteps.*

Figure 4.3 shows the frequency content of other animals, as well as humans. In Figure 4.3c, one can see that humans, being the most similar to the elephant footsteps, has a majority of its frequency content in the 5-40 Hz range. The rhinoceros steps in Figure 4.3d have a wider distribution, with the energy being between 5-100 Hz. Both kulans and camels have the majority of their energy over 100 Hz. Figure 4.4 shows a closer comparison between the different animal footsteps. In it, the same ten footsteps, of each animal have been used to create an average footstep.

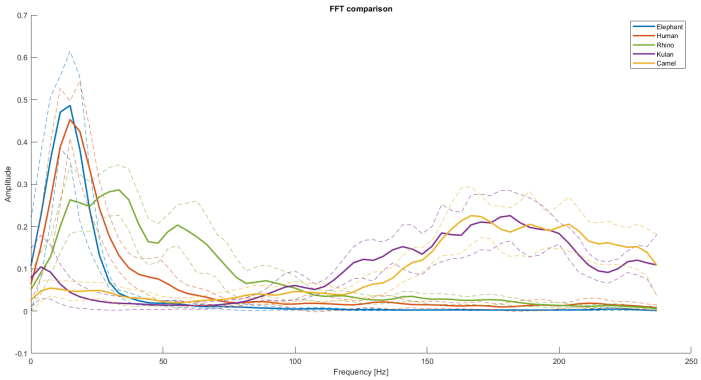

Figure 4.4: *An FFT comparison between elephants, humans, rhinos, kulans and camels. The solid lines represent a mean value of ten footsteps from the animal. The striped lines indicate one standard deviation from the mean.*

Kenya

The datasets presented below are collected from two different locations in Tsavo West. One is waterhole four at Ngulia Rhino Sanctuary, and one at a waterhole outside Kilaguni Serena Lodge.

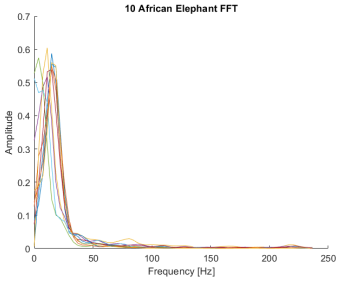

(a) FFT of 10 african elephant footsteps, with a Hamming window, recorded at waterhole four in Ngulia.

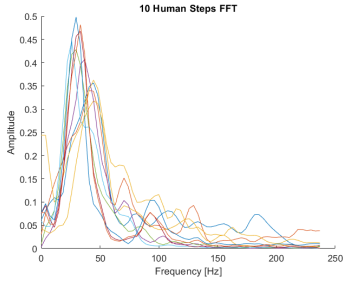

(b) FFT of 10 human footsteps, with a Hamming window, recorded at waterhole four in Ngulia.

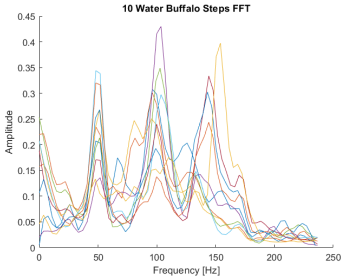

(c) FFT of 10 water buffalo footsteps, with a Hamming window, recorded at a waterhole outside Kilaguni Serena Lodge.

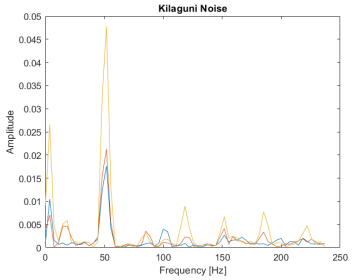

(d) FFT of a segment of 128 samples containing ambient noise, recorded at a waterhole outside Kilaguni Serena Lodge.

Figure 4.5: *FFT from 10 elephant, human and water buffalo footsteps, as well as a segment of ambient noise.*

Figure 4.5a shows that the African Elephant has a majority of its frequency content below 30 Hz. The human footsteps in Figure 4.5b has slightly higher frequencies, with a majority being between 10 - 70 Hz. The water buffalo steps in Figure 4.5c have three distinct peaks at approximately 50, 100 and 150 Hz. Some ambient noise was also noted in this dataset collected at Kilaguni, presented in Figure 4.5d. No ambient noise was noted at the waterhole in Ngulia. In Figure 4.6, averages of the footsteps in Figure 4.5 have been made, and compared in the same graph.

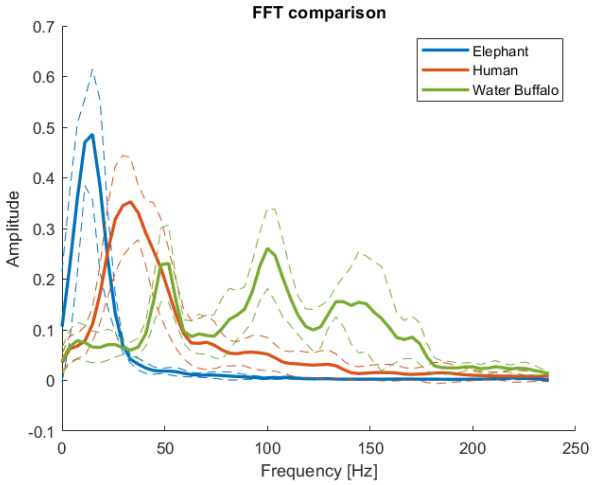

Figure 4.6: *An FFT comparison between elephants, humans, and water buffaloes. The solid lines represent a mean value of ten footsteps from the animal. The striped lines indicate one standard deviation from the mean.*

For comparison purposes later on, some statistics for the signal features on the 10 elephant footsteps in Figure 4.5a were calculated and are presented Table 4.1.

Table 4.1: *Signal feature values, extracted from 10 elephant footsteps collected at Kilaguni.*

Feature	Mean	σ
Frequency peak (Hz)	12.9	3.14
Centroid (Hz)	18.3	3.53
Standard Deviation	0.08812	9.3e-04

4.4.2 Choosing detection parameters

Because there was an abundance of data from Kolmården Wildlife Park, compared to the amount of data from Kenya, the detection algorithm is designed to detect the elephants at Kolmården. The signal feature parameters as well as the average footstep are calculated on 109 footsteps, collected from a single male elephant.

Signal Feature Method

The resulting signal features, as described in Section 4.2.3 are presented in Table 4.2.

Table 4.2: *Signal feature values, extracted from 109 elephant footsteps.*

Feature	Mean	σ
Frequency peak (Hz)	13.2	3.72
Centroid (Hz)	19.1	3.62
Standard Deviation	0.08821	6.5e-04

With the metrics from Table 4.2, thresholds can be set. Three different sets of thresholds are evaluated. The thresholds have been chosen as multiples of the standard deviation, of each respective feature, above and below the mean of the parameters. The resulting thresholds are presented in Table 4.3.

Table 4.3: *Detection thresholds for signal features, with different range from the mean.*

1 standard deviation		
Feature	Low threshold	High threshold
Frequency peak (Hz)	9.48	16.92
Centroid (Hz)	15.48	22.72
Standard Deviation	0.08756	0.08886
1.5 standard deviation		
Feature	Low threshold	High threshold
Frequency peak (Hz)	7.62	18.78
Centroid (Hz)	13.67	24.53
Standard Deviation	0.087235	0.089185
2 standard deviations		
Feature	Low threshold	High threshold
Frequency peak (Hz)	5.76	20.64
Centroid (Hz)	11.86	26.34
Standard Deviation	0.08756	0.08691

The 109 footsteps had a mean kurtosis of 5.6 with a standard deviation of 0.57. Based on this, the high kurtosis threshold was set to 4.3 and the low to 3.5. The high threshold is more than two standard deviations from the mean, which should let through most of the footsteps and at least 97.5% of them. The lower threshold is chosen arbitrarily to a slightly lower threshold than the high threshold. The mean ratio between low and high frequencies was 603.1 with a standard deviation of 478.9. This test is a final test for filtering out bad segments and any high frequency animals that somehow slipped through the other tests. A threshold for the ratio is set to 15 at all times. This is low enough to let through good elephant step segments, while discarding animals with high frequency steps. It is also high enough to not be massively effected by high frequency noise.

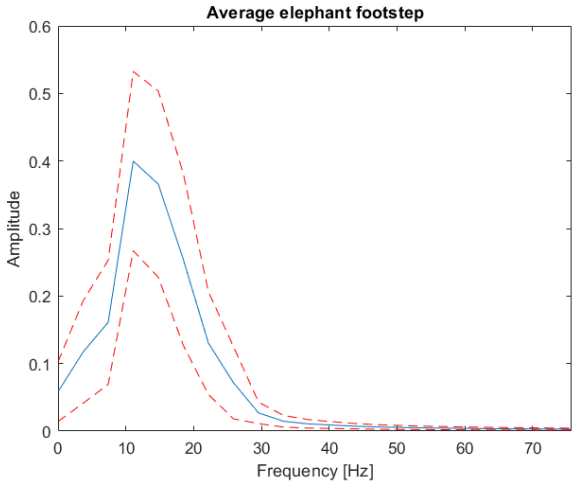

Figure 4.7: *The average FFT of 109 elephant footsteps. The blue line represents the mean value of each frequency, and the red striped line is one standard deviation of the mean.*

Average Footstep

The average elephant footstep was calculated as described in Section 4.3, using the same 109 footsteps as the previous method. The resulting average footstep is presented in Figure 4.7.
Three different threshold values are evaluated, that are two, three and four standard deviations above and below the mean value.

4.4.3 Detection performance

To evaluate the performance of the detection algorithm, video footage was used to count visible footfalls. The performance is only tested on the elephants at Kolmården, and not Kenya. This is because the only elephant data from Kenya already passed through a lighter version of the signal features method on the hardware. Therefore, assessing the performance of the detection algorithms on this data would not be an accurate representation of the actual performance. The performance is assessed in regard to

- *True Positives* (TP) - Detection when an elephant footstep has occurred.
- *True Negatives* (TN) - No detection when something other than an elephant footstep has occurred. No detection on noise is not considered a True Negative.
- *False Positives* (FP) - Detection when no elephant footstep has occurred.
- *False Negatives* (FN) - No detection when an elephant footstep has occurred.

The models will be evaluated by accuracy, calculated in Equation (4.4). The accuracy will give a metric for how many of the classifications made are true. It ranges from 0 to 1 where 1 is the highest accuracy. Recall will also be used, and is calculated with Equation (4.5). This tells how many of the elephant detections gets detected. It ranges from 0 to 1 where 1 is means that all steps are detected. Precision will also be used and is calculated in Equation (4.6). This metric indicates how many of all the detections made are true positives. It also ranges from 0 to 1 where 1 means that all detections are elephants, and 0 is that all detections are other animals. The last metric that will be used is F1 score, and is calculated in Equation (4.7). This is a harmonic mean of the recall and precision of a model. This will give a good overview of the performance of the algorithm. It ranges from 0 to 1 where a high number is good [15].

$$Accuracy = \frac{\mathrm{TP} + \mathrm{TN}}{\mathrm{TP} + \mathrm{TN} + \mathrm{FP} + \mathrm{FN}} \tag{4.4}$$

$$Recall = \frac{\mathrm{TP}}{\mathrm{TP} + \mathrm{FN}} \tag{4.5}$$

$$Precision = \frac{\mathrm{TP}}{\mathrm{TP} + \mathrm{FP}} \tag{4.6}$$

$$F1 = 2\frac{Recall * Precision}{Recall + Precision} \tag{4.7}$$

The models are evaluated on datasets different from the ones that contain the training data. The elephant validation data is taken from a single male elephant, walking about 5-35 meters away. This data was recorded last year by other students. During the data collection for the rhinos, one of the geophones was down, hence the detection criteria are only applied to the two working channels. The footsteps were counted from video footage, to make the amount of missed detections evident. All models have been validated on the same datasets corresponding to each animal. Each animal validation is done in one or more datasets where the geophones have recorded continuous seismic data, containing 57 footsteps of each respective animal, except for the Kulan. Only 49 Kulan footsteps were recorded.

Signal feature method

Table 4.4: *Detection results from different animal footsteps.*

1 standard deviation				
Animal	TP	TN	FP	FN
Elephant	17	0	0	40
Human	0	57	0	0
Rhino	0	57	0	0
Camel	0	57	0	0
Kulan	0	49	0	0
Total	17	220	0	40
1.5 standard deviation				
Animal	TP	TN	FP	FN
Elephant	31	0	1	26
Human	0	57	0	0
Rhino	0	54	3	0
Camel	0	57	0	0
Kulan	0	49	0	0
Total	31	217	4	26
2 standard deviations				
Animal	TP	TN	FP	FN
Elephant	35	0	1	22
Human	0	54	3	0
Rhino	0	53	4	0
Camel	0	57	0	0
Kulan	0	49	0	0
Total	35	213	8	22

Table 4.4 shows the detection results of different animals footsteps. Noteworthy is that the false positive from the elephant data is from in between footsteps. That is, it is from the rumbles of an already detected footstep, resulting in the algorithm detecting the same footstep twice. The accuracy, recall, precision and F1 score of the models are presented in Table 4.5.

Table 4.5: *Detection results from different animal footsteps.*

Standard deviation	Accuracy	Recall	Precision	F1 score
1	0.86	0.30	**1**	0.46
1.5	**0.89**	0.54	0.89	0.67
2	**0.89**	**0.61**	0.81	**0.7**

Average footstep method

Table 4.6: *Detection results from different animal footsteps, for the average footstep method.*

2 standard deviation				
Animal	TP	TN	FP	FN
Elephant	20	0	1	37
Human	0	57	0	0
Rhino	0	57	0	0
Camel	0	57	0	0
Kulan	0	49	0	0
Total	20	220	1	37
3 standard deviation				
Animal	TP	TN	FP	FN
Elephant	34	0	1	21
Human	0	49	8	0
Rhino	0	55	2	0
Camel	0	57	0	0
Kulan	0	49	0	0
Total	34	210	11	21
4 standard deviations				
Animal	TP	TN	FP	FN
Elephant	40	0	3	17
Human	0	40	17	0
Rhino	0	51	8	0
Camel	0	51	12	0
Kulan	0	48	8	0
Total	40	190	48	17

Table 4.6 shows the detection results for the average footstep method. Noteworthy is that the false positives from the elephant data is from in between footsteps. That is, it is from the rumbles of an already detected footstep, resulting in the algorithm detecting the same footstep twice. The rhino, camel and kulan tests all had detections from ambient noise in with 4 standard deviations as threshold. The accuracy, recall, precision and F1 score of the models are presented in Table 4.7.

Table 4.7: *Detection results from different animal footsteps.*

Standard deviations	Accuracy	Recall	Precision	F1 score
2	0.86	0.37	**0.95**	0.53
3	**0.88**	0.60	0.75	**0.67**
4	0.78	**0.70**	0.45	0.55

4.5 Discussion

In this section, the results of the two developed detection algorithms are discussed.

4.5.1 Signal Feature Method

The signal feature method worked quite well. Some animals are easier to differentiate than others. One could come to this conclusion by analysing Figure 4.4 and Figure 4.6. In Figure 4.4, the camel and kulan FFTs have frequencies that are a lot higher, compared to the other three animals. This is directly translated into the results of Table 4.4, where no kulan nor camel footsteps have been detected for any of the thresholds. An unexpected result is that more rhino footsteps were detected than human footsteps. By looking at Table 4.4, one could make the assumption that that would not be the case. One explanation for this could be the fact that one of the geophones was down during these measurements. This means that only two geophones have to detect an elephant instead of three, making false positives more likely.

Just by looking at Table 4.5, one could conclude that the algorithm works best with the thresholds at two standard deviations. It has the highest accuracy, recall and F1 score. However, one could argue that for the elephant detector, it is important to have good precision. If the detectors are deployed in the field, sending information to park rangers, frequent false alarms from human footsteps could mean the rangers stop listening to it, rendering the device useless. Therefore, having two standard deviations as thresholds is too high for the intended purpose. The same could be said about having 1.5 standard deviations as thresholds. It also had some false alarms from rhino footsteps. However, knowing that the rhino tests only were done with two out of three geophones makes these false positives less significant. The rarity of rhinos in the wild also makes it very unlikely to detect one, and if one is detected, this information would also be of importance to the park rangers. Therefore, 1.5 standard deviations seem to be a good tradeoff between recall and precision, giving it a good F1 score, as well as having high accuracy.

Although there is not an abundance of data, by comparing Table 4.1 and Table 4.2, one could draw the conclusion that the detection algorithm would work well for African elephants as well. The metrics are very similar, with the most deviating one being the normalised standard deviation. It is however difficult to come to a certain conclusion about this, since the amount of data is quite lacking.

4.5.2 Average footstep method

The average footstep detection algorithm had some drastic changes when changing the threshold. Three standard deviations as thresholds gave the best F1 score. It did however detect 14 % of the human footsteps. This is reasonable when

comparing to figure Figure 4.4, since human and elephant footsteps are the most similar, and three standard deviations is a quite large threshold. Since the device should prioritise maximising precision, especially when it comes to human footsteps, as the devices' intended locations are close to human settlements, having two standard deviations as thresholds would be the most fitting for the elephant detections.

This detection method could be further improved with more training data. 109 elephant footsteps in not sufficient for making an accurate model of an average elephant footstep. The results do however show promise, and the method could be more viable with more data.

4.5.3 Comparison

The two methods show quite different results, but in general the signal feature method show better accuracy and precision. In Figure 4.8, one can see that the average footstep method tends to have a higher recall, but at the cost of precision. The most appropriate thresholds for the two algorithms, for the intended purpose, were 1.5 standard deviations for the signal feature method and 2 standard deviations for the average footstep. The signal feature method outperforms the average footstep method in all categories, except for when it comes to precision. However, as discussed in Section 4.5.1, the false positives in that data might not be as significant as it looks. Therefore, the signal feature method is the best choice for the hardware implementation of the detection algorithm. It is quite possible that the average footstep method would be a more feasible option, if more data was available.

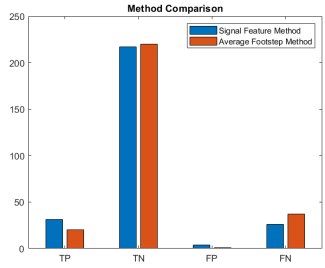

(a) TP, TN, FP and FN comparison between the two methods.

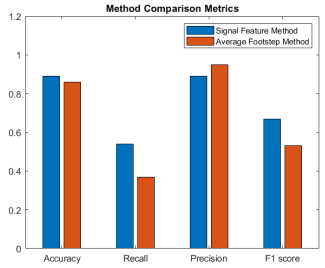

(b) Accuracy, recall, precision and F1 score comparison between the two methods.

Figure 4.8: *Two different comparisons between the two models.*

5

Direction of Arrival and Localisation

This section aims to explain how the DOA estimates are calculated, as well as how multiple geophone arrays can be used to calculate the location of an elephant.

5.1 Signal model

The signal model that is used, is the measured signal $y_i[k]$ for geophone i, which consists of some ambient noise $e_i[k]$ after being filtered in a 2nd order Butterworth high-pass filter, with cutoff frequency of 4 Hz and the seismic signature of an elephant's footstep $s[k]$. The signal model is based on segmentwise data which begin when an elephant footstep is detected and is approximately 270 ms long.

$$y_i[k] = s[k - \tau_i] + e_i[k]$$
$$\tau_i = \delta - D_i(\phi)$$

ϕ is the DOA angle, δ is the time for the footstep when it reaches a reference point, $D_i(\phi)$ is the geometric delay for the seismic signature relative to a reference point, and τ_i is the total delay of the footstep for geophone i.

5.2 Experimental setup

In all experimental setups, the geophones are placed in an equilateral triangle, where each side is $d = 4$ m, see Figure 5.1.

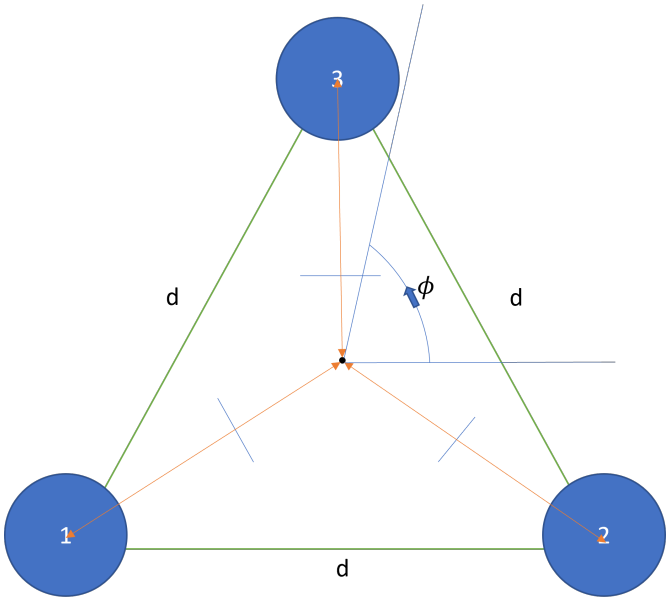

Figure 5.1: *The geophone array illustrated.*

5.3 Wave propagation speed

By detecting a step which is aligned with a geophone pair, the wave propagation speed can be calculated by finding the delay between the geophones. The wave propagation speed becomes, $c = \frac{d}{\tau_{i,j}}$, where $\tau_{i,j}$ is the delay between two geophones which are aligned with the seismic source.

5.4 Geometric delay

A reference point is chosen to be in the middle of the array, at the same distance from each geophone. By using trigonometry, the distance to the reference point can be calculated.

$$\frac{d}{2\cos(30°)} = \frac{d}{\sqrt{3}}$$

When an elephant is detected, a DOA estimation is performed by looking at the geometric delay from each geophone to the reference point. In Figure 5.2 a detection from direction ϕ is illustrated.

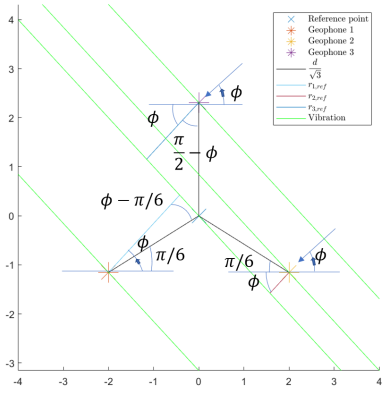

Figure 5.2: *The Figure illustrates the distance ($r_{i,ref}$) a wave travels between a geophone and the reference point from direction ϕ.*

By knowing the speed of the wave, c, and knowing the distance to the reference point, the geometric delay between the reference point and each geophone can be calculated.

$$D_1(\phi) = \frac{r_{1,ref}}{c} \cdot f_s = -\frac{d \cdot \cos(\phi - \frac{\pi}{6})}{\sqrt{3} \cdot c} \cdot f_s$$

$$D_2(\phi) = \frac{r_{2,ref}}{c} \cdot f_s = \frac{d \cdot \cos(\phi + \frac{\pi}{6})}{\sqrt{3} \cdot c} \cdot f_s$$

$$D_3(\phi) = \frac{r_{3,ref}}{c} \cdot f_s = \frac{d \cdot \cos(\frac{\pi}{2} - \phi)}{\sqrt{3} \cdot c} \cdot f_s$$

where f_s is the sampling frequency.

5.5 DOA resolution

The DOA resolution depends on multiple factors. With no modification of the signal, the DOA resolution is quite low, and the solution can be within a great span of angles.

5.5.1 Upsampling

If the signal is upsampled, the maximum delay will increase and thereby also the delay will have a smaller set of possible angles as solutions. The signal is upsampled using cubic splining. Cubic spline is a good method in our case since our signals are seismic waves which oscillate. It is then easy for a cubic spline to match a spline on the oscillations since it is a piecewise cubic polynomial which is twice continuously differentiable [5].

5.5.2 DOA resolution error

The tested angles, ϕ, in the search of finding the DOA, consists of angels from -180° to 179° with a step of one degree between each element. If a signal is upsampled and has unique solutions for all angles, there is still a risk that the solution differs with a maximum of 0.5° from the real solution. If a detection is made from a distance of 100 m from a sensor station, this gives a total error range of $2 \cdot 100 \cdot \tan(0.5) \approx 1.75$ m which is very low when tracking elephants since the length of an elephant is typically up to 5 meters.

5.6 Delay and sum

To estimate the direction of the elephant footstep, delay-and sum is used [27]. The signal model is used to estimate the DOA using Non-Linear Least Squares (NLS).

$$V(\phi) = \sum_{i,j,i\neq j} \sum_{k\in W} (y_i[k - D_i(\phi)] - y_j[k - D_j(\phi)])^2$$

$$\hat{\phi} = \arg\min_{\phi} V(\phi)$$

Where W denotes a sliding time window which consists of a segment of an elephant footstep.

5.7 Confidence interval

The confidence interval will be estimated by looking at the minimum in the cost function. By trying to fit a second order polynomial curve, the variance can be calculated.

$$V(\phi) \approx a + b\phi + c\phi^2$$

The fitting is done on a grid within 20 degrees from the estimated DOA $\hat{\phi}$. Once the polynomial is estimated, the variance can be calculated.

$$\hat{\hat{\phi}} = -\frac{b}{2c}$$

$$V(\hat{\hat{\phi}}) = a - \frac{b^2}{4c}$$

$$\bar{V}(\hat{\hat{\phi}}) = 1 - \frac{b^2}{4ca}$$

$$\mathrm{Var}(\hat{\hat{\phi}}) = \frac{a - \frac{b^2}{4c}}{Nc}$$

Where $\hat{\hat{\phi}}$ is the new DOA estimate and N is the number of samples in the signal [13].

5.8 Triangulation

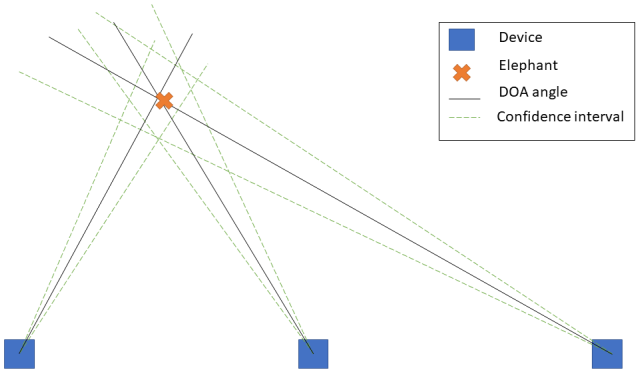

Figure 5.3: *Illustration of the triangulation of an elephant's location, with DOA angles and their confidence intervals.*

Figure 5.3 illustrates the basic principle of the location estimate. With the direction estimates for multiple devices, a NLS estimate of an elephant's location is formulated as

$$\hat{x} = \arg\min_{x} \sum_{m=1}^{M} (\phi_m - \arctan 2(x_y - p_{m,y}, x_x - p_{m,x}))^2 \tag{5.1}$$

where m denotes a specific device, x_y and x_x denotes the location of the elephant in the northern axis respective eastern axis, while $p_{m,y}$ and $p_{m,x}$ denotes device m location in the northern axis respective eastern axis and M is the number of devices that have calculated a DOA of the elephant. With Equation (5.1), a gradient search is used to find the estimate of $\hat{x}$ [12]. The positions of the devices are known by GNSS coordinates converted to Universal Transverse Mercator (UTM).

Additionally, only measurement which is 0.5 seconds away from each other will be used since the sensor stations will be maximum 50 m away from each other and one step should maximumly arrive to another $\frac{50}{c} = \frac{50}{160} = 0.3125 < 0.5$s later.

5.8.1 Boundaries

By using boundaries in the optimisation, the solution will be calculated quicker and be more accurate. The solution can be predicted between some coordinates by looking at the DOA for each device and the device position. Below are the logic for the minimal and maximal possible solutions on the northern-axis, listed with a given detection range r.

- If the most northern device gets a DOA estimate from west or east, see Figure 5.4a, then there will be only one possible solution on the northern-axis which is the northing position of this device. The same applies for the most southern device, illustrated in Figure 5.4b.

- If the most northern device gets a DOA estimate in a northern direction, see Figure 5.4c and Figure 5.4d, the minimum possible solution on the northern-axis is the northing position of this device and the maximum solution on the northern-axis is $\min(p_{1,y} + r \cdot \sin(\phi_1), p_{2,y} + r \cdot \sin(\phi_2))$, where p_1 is the most northern device and p_2 is the most southern device.

- If the most southern device gets a DOA estimate in a southern direction, see Figure 5.4e and Figure 5.4f, the maximum possible solution on the northern-axis is the northing position of this device and the minimum solution on the northern-axis is $\max(p_{1,y} + r \cdot \sin(\phi_1), p_{2,y} + r \cdot \sin(\phi_2))$, where p_1 is the most southern device and p_2 is the most northern device.

- If none of the above cases happens, then should the most southern device have a DOA estimate from a northern direction and the most northern device should have DOA estimate in a southern direction, see Figure 5.4g. The maximum possible solution on the northern-axis is the northing position of the most northern device and the minimum possible solution on the northern-axis is the northing position of the most southern device.

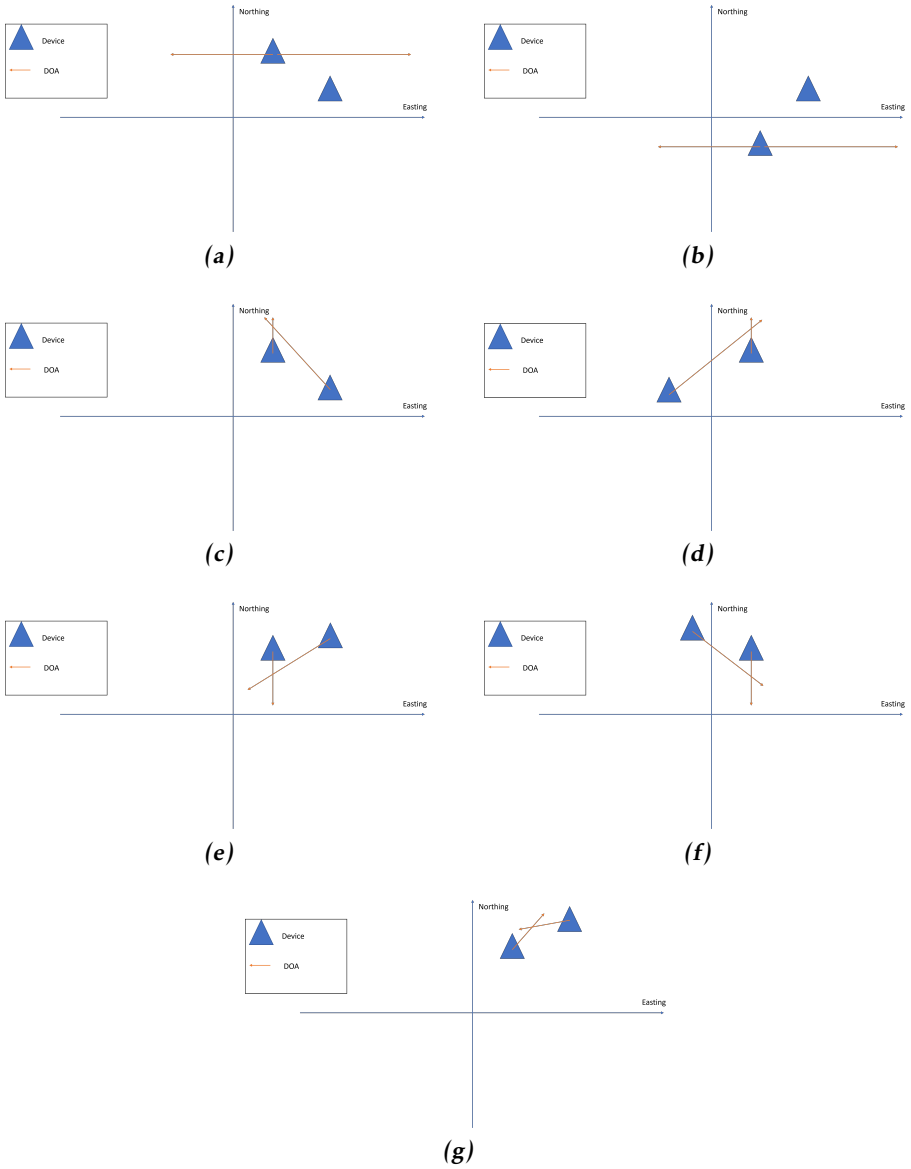

Figure 5.4: *Visualisation of possible northing positions given DOA estimates.*

Similar logic applies to the boundaries on the eastern-axis which are listed below.

- If the most eastern device gets a DOA estimate from north or south, see Figure 5.5a, then there will be only one possible solution on the eastern-axis which is the easting position of this device.

- If the most western device gets a DOA estimate from north or south, see Figure 5.5b, then there will be only one possible solution on the easting-axis which is the easting position of this device.

- If the most eastern device gets a DOA estimate in an eastern direction, see Figure 5.5c and Figure 5.5d, then the minimum possible solution on the eastern-axis is the easting position of this device and the maximum solution on the eastern-axis is $\min(p_{1,x} + r \cdot \cos(\phi_1), p_{2,x} + r \cdot \cos(\phi_2))$, where p_1 is the most western device and p_2 is the most eastern device.

- If the most western device gets a DOA estimate in a western direction, see Figure 5.5e and Figure 5.5f, then the maximum possible solution on the eastern-axis is the easting position of this device and the minimum solution on the eastern-axis is $\max(p_{1,x} + r \cdot \cos(\phi_1), p_{2,x} + r \cdot \cos(\phi_2))$, where p_1 is the most western device and p_2 is the most eastern device.

- If none of the above cases happens then should the most eastern device have a DOA estimate from a western direction and the most western device should have DOA estimate in an eastern direction, see Figure 5.5g,. The maximum possible solution on the eastern-axis is the easting position of the most eastern device and the minimum possible solution on the eastern-axis is the east position of the most southern device.

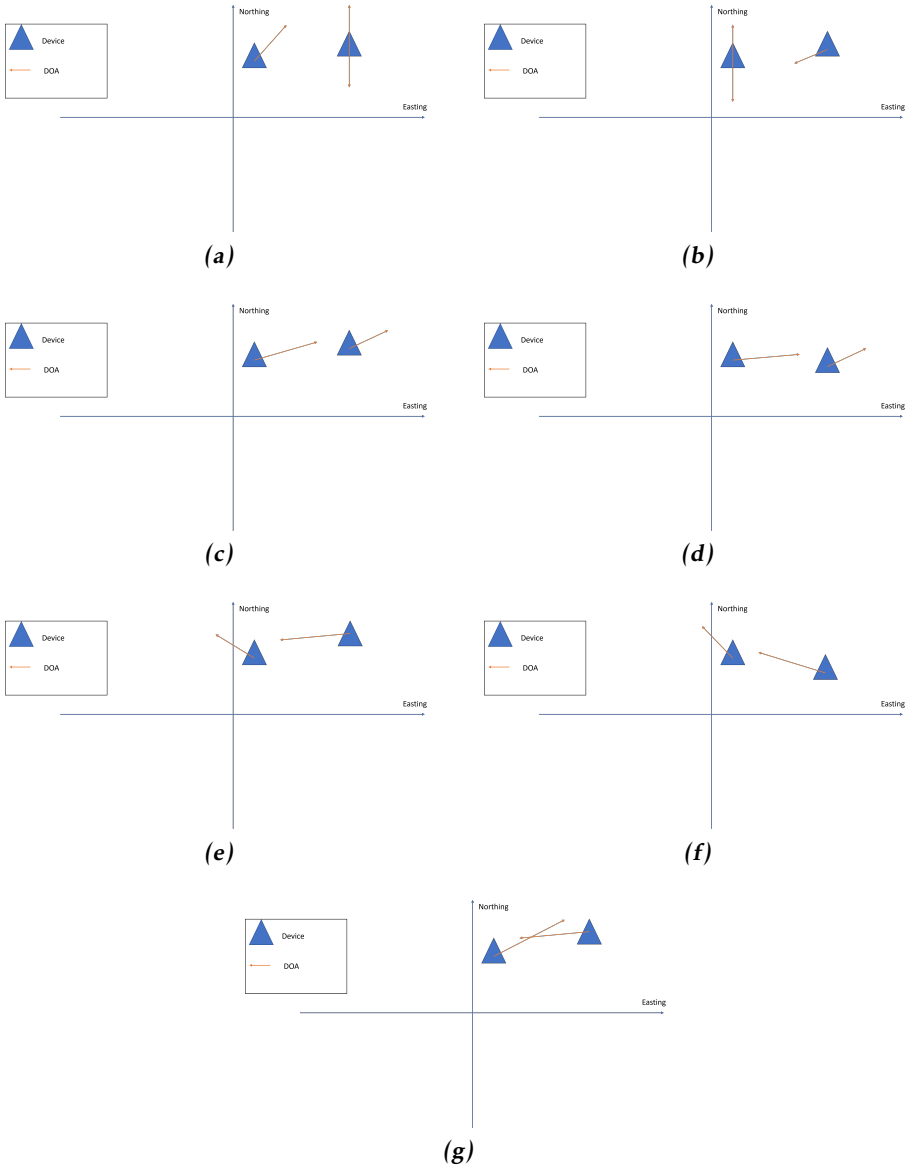

Figure 5.5: *Visualisation of possible easting positions given DOA estimates.*

There are also cases when there is no intersection inside the boundaries. This will happen when a pair of measurements have an intersection but not inside the shared detection range of the devices. This means that measurements comes from different sources and will get a solution where no object exists. By using boundaries, the given solution will get a high cost and can be easily filtered out.

5.8.2 Reasonable measurements

There will be cases where the algorithm tries to find an intersection between two measurements, but in reality there is no intersection. This will lead to a solution with high cost and long computational time. To save time and avoid trying to find a solution in these cases, one can predict if there should be a solution to the optimisation problem before optimising. If one of the listed cases below occur, no triangulation will be performed.

- If the most southern device gets a DOA estimate in a southern direction and the most northern device doesn't, no solution will be found.
- If the most northern device gets a DOA estimate in a northern direction and the most southern device doesn't, no solution will be found.
- If the most eastern device gets a DOA estimate in an eastern direction and the most western device doesn't, no solution will be found.
- If the most western device gets a DOA estimate in a western direction and the most eastern device doesn't, no solution will be found.
- If the two devices have the same northing positions, has DOA estimates from in either a southern or northern direction and the most western device has a greater absolute value of DOA than the other device, see Figure 5.6, no solution will be found.
- If the two devices have the same northing positions and one gets DOA estimates in a southern direction and the other doesn't, no solution will be found.

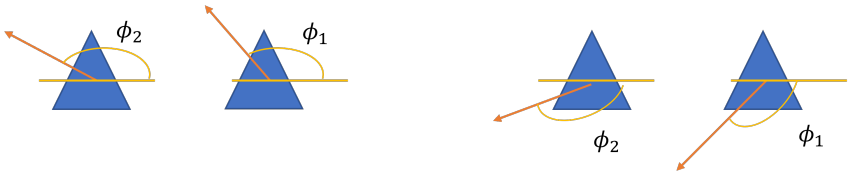

Figure 5.6: *Illustration of when no intersection happens for two aligned devices in the eastern direction.*

5.9 Result

In this section, results regarding the methods for DOA and triangulation are presented. The DOA estimates are validated using a 360insta ONE x2 camera. This camera is able to record video in 360 degrees. The camera is then placed in the middle of a geophone array. Three metal poles are hammered in the ground to visualise the geophone locations. These also act as reference angles in the video footage. The footage is projected using a equirectangular projection, to keep the

angles from the video true to the real angles. A grid can then be applied to the video to aid the validation of the angles.

5.9.1 Wave propagation speed

After collecting data on elephants in Kolmården, data was also collected for calculating the wave propagation speed. The wave propagation speed was calculated by 10 different measurements. The mean value for wave propagation speed became 161.7 m/s with a standard deviation of 12.3 m/s. In Figure 5.7 a histogram shows how the measurements are distributed.

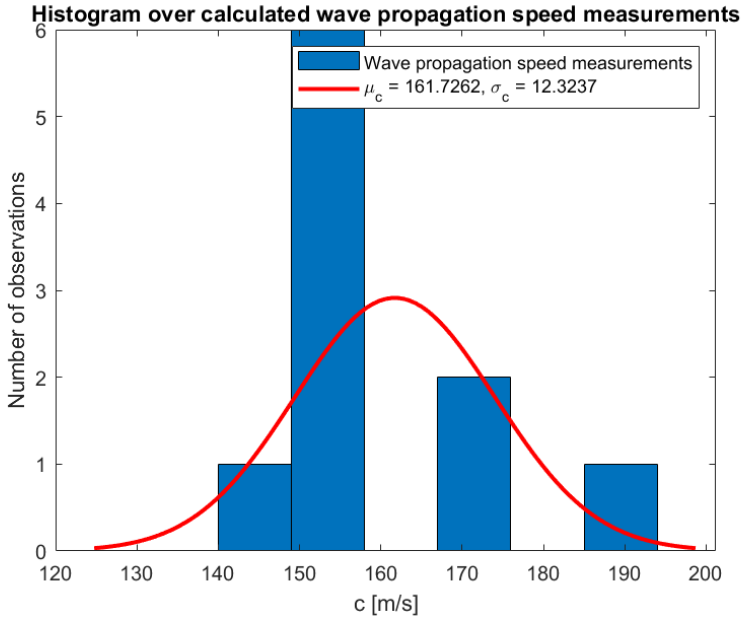

Figure 5.7: *A histogram for collected wave propagation speed measurements with a normal distribution fit.*

Most of the measurements are distributed around the mean value, while one outlier of 188 m/s brings up the standard deviation drastically. Similar results of the wave propagation speed have been seen for measurements in other locations in Sweden, as Vallamassivet.

5.9.2 Upsampling

After testing out different sampling frequencies with cubic splining for the signals, upsampling the original 474 Hz signal to 4000 Hz has been shown to give a result where each angle between -180 to 179 degrees with a step of 1, give a unique solution to the DOA cost function, see Figure 5.8. That is, no two angels share the same solution.

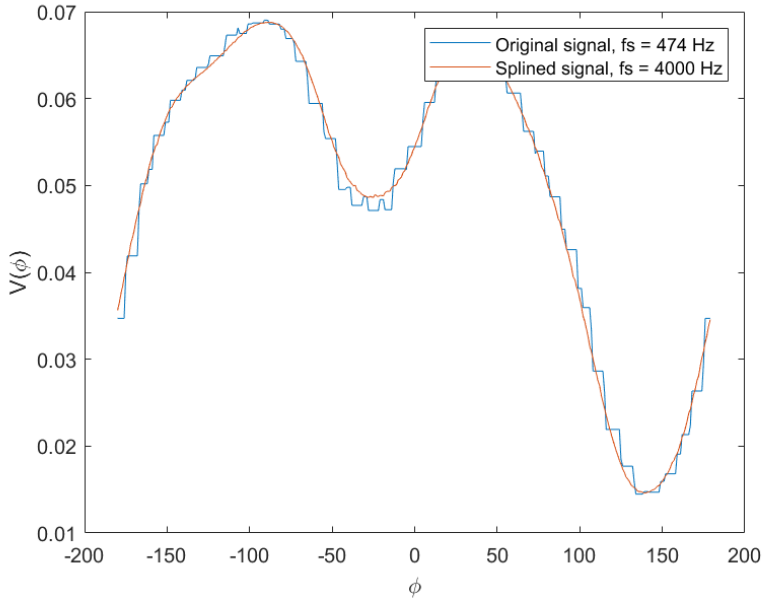

Figure 5.8: *Comparison of the cost functions for the original signal and a splined signal.*

5.9.3 Variance estimation

In Figure 5.9, 4 different DOA cost functions are shown for 4 different detections. The cost functions are chosen to present the variety of how the DOA cost functions can look. All 4 cost functions does have a global minimum but of different qualities and the DOA estimate $\hat{\phi}$ can be told to be in an interval of 2 standard deviation away from the $\hat{\hat{\phi}}$ with a probability of 95 %. The least squares (LS) second order polynomial fit does also seem to fit all cost functions with the chosen grid for respective cost function and the calculated variance seems reasonable when looking at how fast the cost changes near the global minimum.

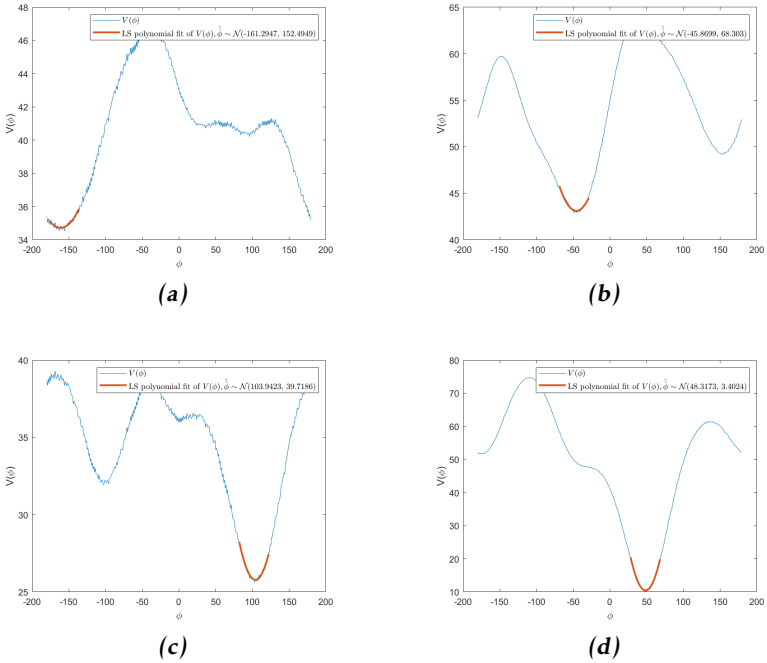

Figure 5.9: *4 different DOA cost functions with matched LS second order polynomial fitted curves*

In Figure 5.10 is the distribution for the difference between the DOA measurement $\hat{\phi}$ from delay and sum and the DOA estimates $\hat{\hat{\phi}}$ from the variance estimation shown. Both estimates are quite close to each other overall and 90 % of the DOA measurements has a maximum difference of 2.6° from the new estimation where the variance is estimated. Since the difference between the two DOA measurements is quite low, the DOA estimate from delay and sum is approximated to have the same measurement variance as $\hat{\hat{\phi}}$.

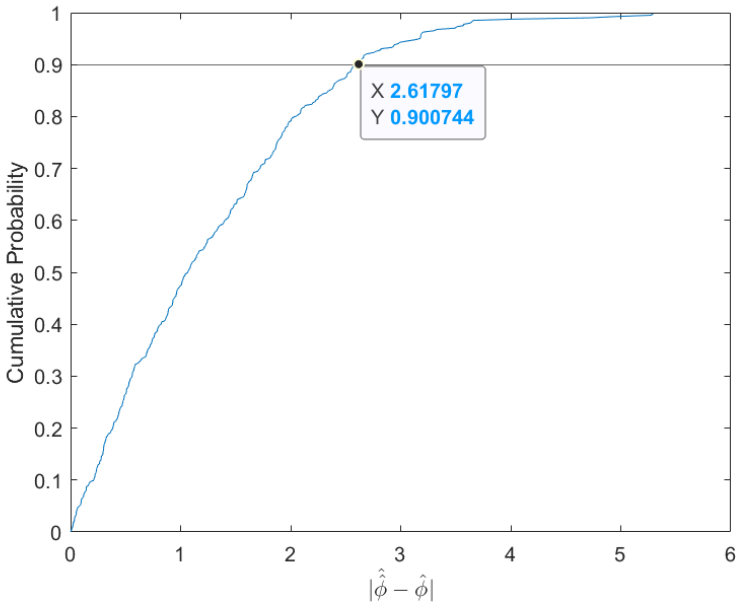

Figure 5.10: *Cumulative distribution function of the distance between the DOA measurements from delay and sum and the DOA estimates $\hat{\hat{\phi}}$ from the variance estimation.*

All further mentions of DOA measurements are DOA estimates from delay and sum with a measurement variance estimated by this section's calculations.

5.9.4 DOA variance threshold

During a 15-minute-long recording, of an elephant walking, a total of 404 elephant footsteps were detected from two devices. In Figure 5.11 the cumulative probability for the variance is shown, noticeable are there no DOA measurements with a variance under 0 which indicates all estimates are minimums. When accepting measurements with a variance under approximately 25, 91% of the measurements will be accepted. The DOA variance threshold is chosen as 25 since the measurements will have a quite low measurement variance for the tracking filters and also to get rid of the measurements with unclear global minimums and probably poor estimates.

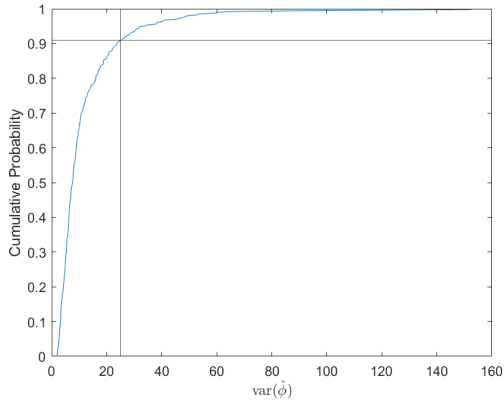

Figure 5.11: *Cumulative distribution function of our DOA variances.*

5.9.5 DOA measurements

In Figure 5.12 DOA measurements from a walking elephant at Kolmården can be seen. The measurements are validated for all the elephant steps except the steps between approximately 10 and 30 degrees where a bush stood, Also, which was discussed in, Section 5.9.4 only measurements with a variance below 25 are shown.

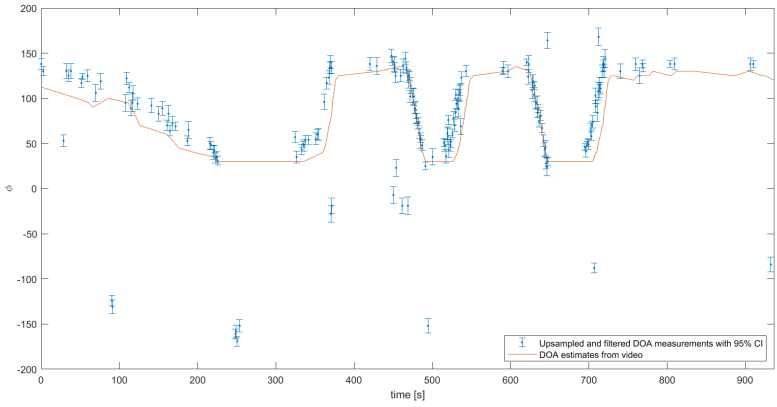

Figure 5.12: *DOA measurements of a walking elephant at Kolmården.*

5.9.6 Triangulation

From the same data collection as the DOA measurements were calculated on, triangulation can also be done. These results are harder to validate since only one camera was available and only one sensor station's DOA measurements could be

validated. Although from our observations the elephant moved back and forth in the eastern direction and the elephants had almost a constant northing position with a possible variation of 17.5 m, a minimum of 2.5 m and maximum of 20 m and a minimum of -13 m and maximum of 30 m in easting position based on satellite pictures, see Figure 5.13.

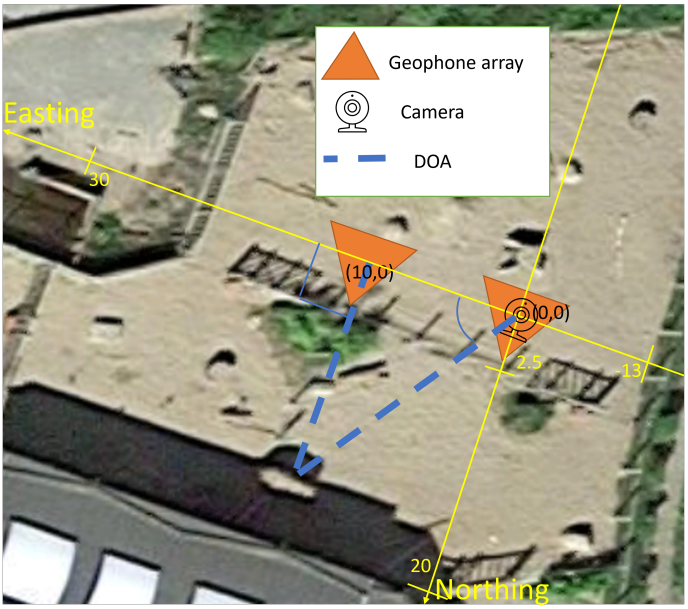

Figure 5.13: *Visualisation of the experimental setup at Kolmården.*

By these observations, an estimate of the elephant's localisation is made by assuming that the elephant has a constant position northing position which is almost in the middle of the two parallel fences in the eastern direction. The estimate for the northing position becomes, then, 2.5 + 9 = 11.5 m. By this assumption and knowing the DOA, an estimate of the easting position can be done. By comparing the northing position with the DOA estimates from the video, a distance to the elephant can be calculated, $\left|\frac{x_y}{\sin(\phi)}\right|$. By knowing the distance to the elephant and the DOA, the easting position can easily be calculated, $x_x(\phi) = \left|\frac{x_y}{\sin(\phi)}\right| \cdot \cos(\phi)$. Important to remember is that the DOA measurements are only validated down to 30 degrees, which was discussed in Section 5.9.5 and therefore is the maximum easting position from the video estimates $x_x(30) \approx 19.9$ m but in reality should there be easting estimates up to 30 m.

Discussed in Section 5.8, 0.5 s were distinguished as a good maximum time difference between two sensor stations measurements. For our data does this time difference give very few localisation estimates though and therefore is a time difference of 2 s is used instead. Bigger time differences give more localisation es-

timates, but important to keep in mind is that the risk of poor estimates may increase since the risk of that the measurements comes from different footstep increases.
In Figure 5.14 northing estimates can be seen for a time difference of 2 s. 49.3 % of the estimates are inside the northing boundary. In Figure 5.15 the easting estimates can be seen for a time difference of 2 s. 90.9 % of the estimates are inside the easting boundary. 48.6 % of the estimates were inside both of the easting and northing boundaries. 142 localisation estimates could be done while each sensor station number of DOA measurements were 148 and 177, respectively.

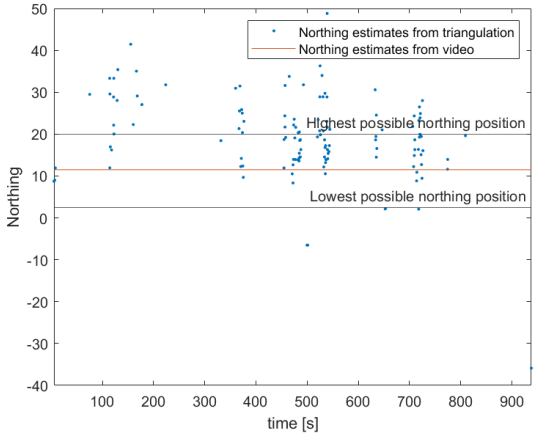

Figure 5.14: *Northing estimates of a walking elephant at Kolmården with a maximum time difference of 2 seconds between the paired measurments.*

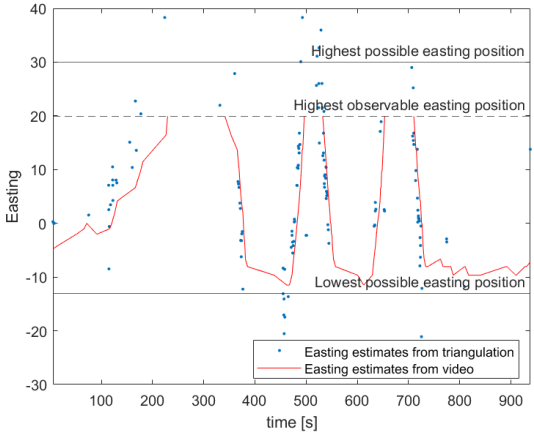

Figure 5.15: *Easting estimates of a walking elephant at Kolmården with a maximum time difference of 2 seconds between the paired measurements.*

5.10 Discussion

In this section, the presented results about DOA and triangulation are discussed.

5.10.1 DOA

From the results in Figure 5.12, it can be said that the DOA measurements is being pretty good estimated. The measurements are close to the validation, but not exactly the same. The difference can come from many factors. One is that the camera is not exactly centred, and thereby, the DOA estimates from the video will not be 100 % correct. A second reason could be that the geophones are not placed 100 % as the experimental setup, and thereby the DOA measurements will not be as expected. Another reason may be that the upsampling is not good enough and the real solution can not be found because of that. Although the DOA estimates from the upsampled versus the non upsampled detections are quite similar, see Figure 5.16, and the upsampling shouldn't give worse solutions at least which can be seen in Figure 5.8.

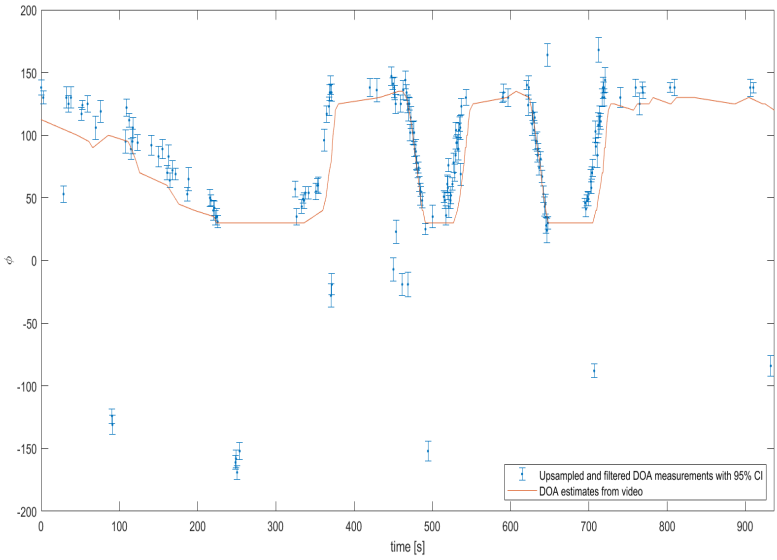

(a) *DOA measurements for a splined signal with sampling frequency 4000 Hz.*

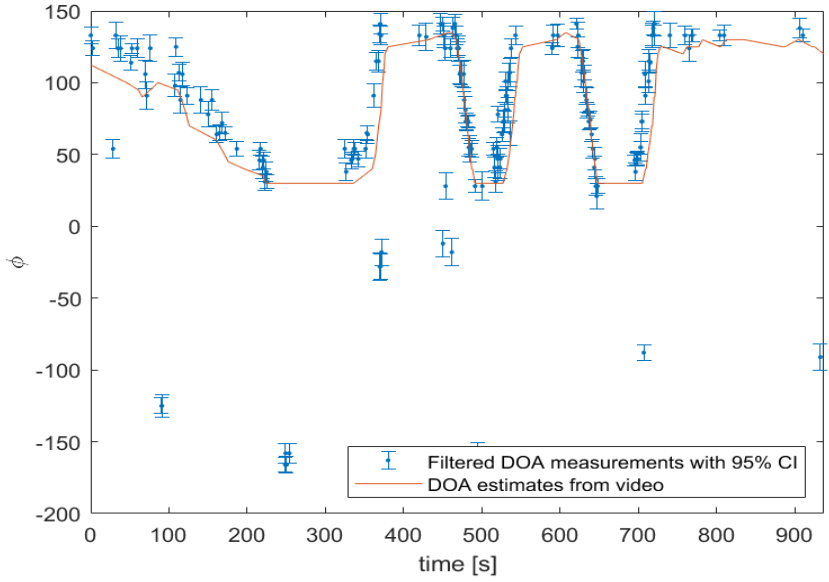

(b) *DOA measurements for the original signal with sampling frequency 474 Hz.*

Figure 5.16

Another thing to discuss is the variance. All the presented measurements has

a variance below 25 and thereby a standard deviation of 5. This means that all measurements has a probability of 95 % to be within two standard deviations from the real solution. By looking at the results again, this seems reasonable. The measurements which are a bit off from the validation are often not much more than 10 degrees away from these measurements. There are also measurements which are far from the validation, but the number seems to be quite low. These measurements will also be handled in the tracking and will be not be associated with a track and thereby will be no problem since they are few and not so frequent. Why these measurements exists can depend on various reasons. One is that the detection algorithm doesn't have to get perfect segment for DOA estimation when detecting elephants, and thereby may the detection not always be suitable for DOA estimation.

5.10.2 Triangulation

In Figure 5.14 and Figure 5.15 are DOA measurements with a maximum time difference of 2 seconds triangulated.

By looking at the eastern estimates, one can see that the easting estimates are quite close to the estimates from the video. Although the easting estimates could only be estimated up to 19.9 m which was discussed in Section **??**. In reality, the elephant mostly walked up to 30 m and then turn back and walk in the opposite direction. This can be seen in the measurements as well, where the estimates from the video are constant but the measurements increases to 30 and then decreases to 19.9 m again.

The elephant movement in the northern axis is both harder to validate and estimate. Many of the estimates are outside the boundary of physical possible northing position (outside fence) and most often too high. Also, the northing position varies much faster and more often than the easting positions. Why this happens is hard to say, one reason could be the uncertainty of the DOA measurements. In Figure 5.17, an uncertainty is added to DOA measurements to visualise how uncertainty in the DOA estimations affect uncertainty in the localisation. One can see that for Figure 5.17a and Figure 5.17b, where the target is in front of the devices, the localisation uncertainty is greater in the northern-axis. In Figure 5.17c, where the target is quite far out to the right, the uncertainty starts getting greater in the eastern-axis. In the measurements from Kolmården, the elephant mostly walked in front of the devices, and this effect could therefore mean that errors in the DOA estimations affect the northing coordinate more than easting.

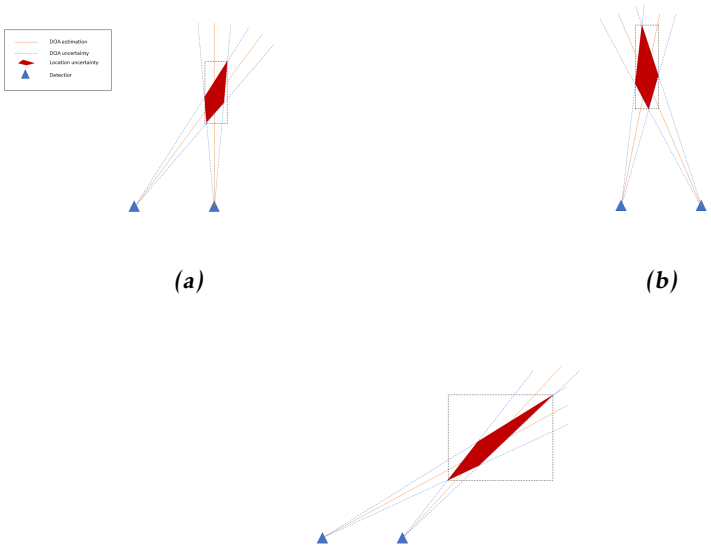

Figure 5.17: *Visualisation of how uncertainty affects easting and northing for different angles.*

One other reason could be poor pairing of DOA measurements. By pairing measurements from different footsteps, the localisation will get poorly estimated. Although it does seem like the northing position is extra sensitive to precise DOA measurements compared to the easting position by the results to judge.

6

Tracking

To keep track of an elephant, various types of Kalman filters can be used. With a Kalman filter, the state can be updated even if there is no measurement, and an elephant can then be tracked even if there are no measurements for a short period of time. This is great for when an elephant is far away from the geophones, and the filter can then predict the movement if the elephant would go out of range. Since the system contains multiple geophone arrays, a Kalman filter can be implemented for each array to update the DOA and an EKF can be implemented to update the positions of the elephants.

6.1 Kalman filter

A Kalman filter does mainly two things. It takes in a measurement and updates the state (measurement update) with respect to the measurement noise. It can also predict the state with a motion model, which calculates the movement since the last measurement (time update). For this, a motion model and measurement model is needed to predict the movement and control the update.

6.1.1 Kalman filter

A Kalman filter is based on a linear state space model, where the general state space models looks as follows.

$$\begin{aligned} x_{k+1} &= F_k x_k + G_{v,k} v_k, & Cov(v_k) &= Q_k \\ y_k &= H_k x_k + e_k, & Cov(e_k) &= R_k \\ Cov(x_0) &= P_{1|0} \\ E(x_0) &= \hat{x}_{1|0} \end{aligned}$$

where x_k is the state, y_k is the measurement, e_k is the measurement noise and v_k is the process noise. F_k is the state transition matrix, H_k is the observation matrix and $G_{v,k}$ is the process noise matrix. In the update there are some matrices that occur multiple times and also says a lot about the measurement and the track. The innovation

$$\epsilon_k = y_k - H_k \hat{x}_{k|k-1}$$

and the innovation covariance

$$S_k = H_k P_{k|k-1} H_k^T + R_k$$

and lastly the Kalman gain

$$K_k = P_{k|k-1} H_k^T (H_k P_{k|k-1} H_k^T + R_k)^{-1}$$

are three of the more frequent terms in the updates. When there is a measurement, a measurement update is performed as follows

$$\begin{aligned} \hat{x}_{k|k} &= \hat{x}_{k|k-1} + K_k \epsilon_k \\ P_{k|k} &= p_{k|k-1} - K_k S_k K_k^T \end{aligned}$$

and the time update for the KF is done as follows

$$\begin{aligned} \hat{x}_{k+1|k} &= F_k \hat{x}_{k|k} + G_{u,k} u_k \\ P_{k+1|k} &= F_k P_{k|k} F_k^T + G_{v,k} Q_k G_{v,k}^T \end{aligned}$$

[12].

6.1.2 EKF

An Extended Kalman Filter is used like a KF, but on a non-linear system. The dynamics are linearised to get an estimate of the mean and covariance of the state. An EKF is based on a nonlinear state space model as

$$\begin{aligned} x_{k+1} &= f(x_k, v_k), & Cov(v_k) &= Q_k \\ y_k &= h(x_k, u_k, e_k), & Cov(e_k) &= R_k \\ Cov(x_0) &= P_{1|0} \\ E(x_0) &= \hat{x}_{1|0} \end{aligned}$$

where e_k is the measurement noise and v_k is the process noise. The state update is performed as described in Section 6.1.4 for respective motion model. In the filter there are some additional terms which has not been stated yet. The innovation for an EKF is

$$\epsilon_k = y_k - h(\hat{x}_{k|k-1}, u_k, 0)$$

, the innovation covariance becomes

$$S_k = H(\hat{x}_{k|k-1}, u_k)P_{k|k-1}(H(\hat{x}_{k|k-1}, u_k))^T + R_k$$

where H is the derivative of h, with respect to x. Lastly the Kalman gain becomes

$$K_k = P_{k|k-1}(H(\hat{x}_{k|k-1}, u_k))^T S_k^{-1}$$

The measurement update becomes

$$\begin{aligned}\hat{x}_{k|k} &= \hat{x}_{k|k-1} + K_k \epsilon_k \\ P_{k|k} &= P_{k|k-1} - K_k S_k K_k^T\end{aligned}$$

and the time update becomes

$$\begin{aligned}\hat{x}_{k+1|k} &= f(\hat{x}_{k|k}, 0) \\ P_{k+1|k} &= F(\hat{x}_{k|k})P_{k|k}F_K^T + G_{v,k}Q_K G_{v,k}^T\end{aligned}$$

where F is the derivative of f with regard to x. [12].

6.1.3 Model and measurement noise

The measurement noise variance can be estimated using the method from Section 5.7. By changing the levels of the process noise, the Kalman filter can be tuned to depend on the measurements or the motion model differently. The process noise does also affect how fast the uncertainty increases for the track. While the uncertainty grows, the probability of letting through new measurements also grows and the risk of updating with false measurement to a track increases. This is discussed more in Section 6.2.4.

6.1.4 Motion model

Motion models are used to predict the movement of a target. A constant position (CP) motion model updates the target's position as constant and if no measurement is present the target will be still.

$$\begin{aligned}x_{k+1} &= F_k x_k + G_{v,k} v_k \\ F_k &= I_n \\ G_{v,k} &= T I_n\end{aligned}$$

A constant velocity (CV) motion model updates the target's position with respect to the estimated velocity, and keeps the velocity constant if no measurement is present.

$$\begin{aligned}x_{k+1} &= F_k x_k + G_{v,k} v_k \\ F_k &= \begin{pmatrix} I_n & T I_n \\ 0 & I_n \end{pmatrix} \\ G_{v,k} &= \begin{pmatrix} \frac{T^2 I_n}{2} \\ T I_n \end{pmatrix}\end{aligned}$$

where T is the time since the last measurement update and n represents the dimension of the state.

6.2 Tracking

This section describes the tracking methods used.

6.2.1 DOA tracking

For the DOA tracking, a traditional Kalman filter is implemented based on a linear state space models with the state $x_k = \begin{pmatrix} \phi_k \end{pmatrix}$ for the CP model and $x_k = \begin{pmatrix} \phi_k \\ \omega_k \end{pmatrix}$ for the CV model. The measurement model becomes

$$y_k = x_k + e_k$$

for the filter with the CP model and

$$y_k = \begin{pmatrix} 1 & 0 \\ 0 & 0 \end{pmatrix} x_k + e_k$$

for the filter with the CV model. The state $\hat{x}_{1|0}$ position is initialised with the first measurement and the covariance $\hat{P}_{1|0}$ is initialised with an arbitrarily high value since no information is available about the track.

6.2.2 Position tracking

Two different filters have been tested out while tracking the position, one based on separate DOA measurements and one based on triangulated DOA measurements.

Separate DOA measurements

This filter is based on separate DOA measurements and depending on from which array the measurement comes from, the used array's position will be the input for the update. The measurement model is a bearing only problem and looks like this,

$$y_k = \operatorname{atan2}(x_{k,y} - p_{k,y}, x_{k,x} - p_{k,x}) + e_k \tag{6.1}$$

where p_k is the input and position of the array k. Since the measurement model is nonlinear, an Extended Kalman Filter is used.

The state is $x_k = \begin{pmatrix} x_{k,x} \\ x_{k,y} \end{pmatrix}$ and the filter uses a CP motion model. The state $\hat{x}_{1|0}$ is initialised with measurements from two arrays, where the measurements are triangulated together as in Section 5.8 to get an initial position. The covariance $P_{1|0}$

is initialised with a high value, since no information is available about the track. Additionally, does the derivate of the measurement model need to be calculated

$$H(x_k, u_k) = h'_x(x_k, u_k, e_k) = \frac{\partial h(x_k, u_k, e_k)}{\partial x_k} = \frac{1}{(x_{k,y} - p_y)^2 + (x_{k,x} - p_x)^2} \begin{pmatrix} -(x_{k,y} - p_y) \\ x_{k,x} - p_x \end{pmatrix} \hat{x}_k$$

Triangulated DOA measurements

For the position tracking using triangulated DOA measurements, a traditional Kalman filter is implemented based on a linear state space models with the state $x_k = \begin{pmatrix} x_{k,x} \\ x_{k,y} \end{pmatrix}$
, measurement model

$$y_k = \begin{pmatrix} 1 & 0 \\ 0 & 1 \end{pmatrix} x_k + e_k$$

and a CP motion model. The state $\hat{x}_{1|0}$ position is initialised with the first measurement and the covariance $\hat{P}_{1|0}$ is initialised with an arbitrarily high value since no information is available about the track.

6.2.3 Measurement

For both of the filters, the DOA is the measurement. The DOA is an angle and is estimated within $-180 \leq \phi < 180$. In the DOA tracking filter, the filter may track one object while the object's DOA goes from 179 to -180. This would give the filter a big innovation and the track would get very uncertain. To avoid that, the measurement is instead recalculated so the distance between the measurement and the filter's estimated DOA is less than 180 degrees, since this is the biggest possible distance between two angles. The recalculation is done by either adding or subtracting a factor of 360 degrees until the distance is below 180 degrees. In the position tracking filter, similar recalculations are also done for the innovation.

6.2.4 Gating

To keep a track relevant, a track should only be updated with new measurements if the measurement is likely to belong to the track. By comparing the prediction of a track with the new measurement and looking at the uncertainty of the track, the measurement can be associated to the track with a given probability. This method is called gating.

Elliptical gating

Elliptical gating compares the distance between the prediction of the target and the new measurement and decide if the measurement belongs to the track or not, given the innovation covariance of the track. By looking at the innovation

covariance of the track, a probability of accepting the measurement through the gate can be calculated. Since the innovation is

$$\epsilon_t = y_t - \hat{y}_{t|t-1} \sim \mathcal{N}(0_{n_y}, S_{t|t-1})$$

and a new term can be expressed as

$$\|\tilde{\epsilon}_t\|_2^2 = \epsilon^T S_{t|t-1}^{-1} \epsilon_t$$

where

$$\tilde{\epsilon}_t \sim \mathcal{N}(0_{n_y}, I_{n_y})$$
$$\gamma = \|\tilde{\epsilon}_t\|_2^2 = \sum_i \tilde{\epsilon}_{i,k}^2 \sim \mathcal{X}(n_y)$$

the probability of accepting the measurement through the gate can then be calculated as

$$P_G = P_r(\gamma \leq \gamma_G) = \int_0^{\gamma_t} \mathcal{X}(\gamma; n_y) d\gamma \tag{6.2}$$

where γ_G is the gate threshold and tells how big the gate is

$$\epsilon_t^T S_t^{-1} \epsilon < \gamma_G$$

[11].

Localisation gating

A positioning track should not be able to be updated by a measurement from a sensor station which has a great distance between the sensor station and the target's estimated position. Therefore, are measurements from sensor stations which are further than $1.5 \cdot r$ m away from the estimated position rejected, where r is the detection range. By giving a marginal of 1.5 times the detection range, a measurement can still be associated with a track which is far away and a badly estimated track can then be readjusted and corrected.

6.3 Multi target tracking

To be able to track multiple targets, there must be some logic deciding when to start tracking a new target, and when to stop tracking a target. A track can either be tentative, confirmed, or dead. A tentative track is a possible track but not decided yet, a confirmed track is considered as a track and a dead track is a track no longer present. A measurement can either initiate a new confirmed or tentative track or update a confirmed or tentative track.

6.3.1 Track logic

To decide when a track is confirmed or should be deleted, one must think about how an elephant behaves. In Section 2.2.1 facts about elephant lifestyle, family constellation and habits are listed. In the same section, observations on the elephants from Kolmården are listed. As described in that section, elephants does eat a lot. A day for an elephant is full of both finding and eating food. For the tracking this means that when an elephant is moving it is likely on the hunt for food and will take many steps on a row. A track should be confirmed when it is likely to have more measurements and have had many measurements. From our collected data, it can be seen that when an elephant moves, our system gives at least 7 detections in a row each time the elephant move. To be able to gather a decent amount of tracks and still being sure that an actual elephant is being tracked, a still alive track is confirmed when it has got 7 measurements.

To keep the complexity of the tracking system down, the alive tracks should only be alive when they get new measurements which are likely to belong to the track. If tracks are not deleted, there is a risk that multiple tracks may share the same information or that a measurement is associated with the wrong track. A track is deleted when the track has not got a measurement in a long time. It is deleted because the uncertainty of a track grows by time, and thereby a track is more likely to accept measurements which does not belong to the track by time. From observations of real elephants, we noted that when an elephant finds food, it does not move much. So if a track does not get new measurements, either the elephant have gone out of range from our sensors, or it is eating. In both of these cases, the track should be kept alive until the uncertainty gets too big. For the case when the elephant has stopped for eating, the track's uncertainty will grow and the probability of accepting a measurement which does not belong to this elephant increases and therefore the track should be deleted. The same logic of deleting track applies to when the elephant goes out of range. Although, these tracks should be kept as long as possible to keep the interesting information from these tracks. From our observations we have seen that when an elephant stops it will either start moving in the nearest 15 seconds again or not move in minutes. Therefore, a track is deleted if it has not got a new measurement after 15 seconds.

6.3.2 Association

To keep the complexity down of the tracking system, a maximum of one track should be updated per measurement. If multiple track are updated with the same measurement, the tracks will be cluttered together and converge into the same track by time. Instead, if a measurement passes through multiple gates from different tracks, there must be a decision to decide where the measurement is most likely to belong to. Firstly, the complexity needs to be low, and therefore the confirmed tracks are prioritised in the association step. If the measurement does not belong to any confirmed track, the measurement can be used to update a tentative track instead. To associate a measurement to one track, the global nearest neighbour algorithm is used, which associates the measurement to the

track with the closest prediction. If a measurement does not seem to belong to any existing track, a new tentative track is initiated with the measurement [11].

6.4 Result

In this section, the two tracking systems for DOA and positioning will be evaluated.

6.4.1 DOA tracking

The DOA tracking system was mainly tuned by two parameters, the model noise and the gating threshold. In the data collection two sensor stations were used but only one of them could be validated since only one 360 camera was available. The KF was mainly tuned to fit the DOA estimates from the video, but also change in a reasonable speed and pattern. Also, as discussed in Section 5.9.4, only measurements with a variance below 25 are used.

Single target

The following results are collected at Kolmården on one elephant. In the data collection, the elephant walked back and forth in front of the sensor stations and the changes in the DOA should almost be linear while the elephant is moving on the same distance.
In Figure 6.1, Figure 6.2, Figure 6.3 and Figure 6.4 the KF estimates can be seen. The KF estimates consists of both measurements and time updates. The KF estimates consists of multiple tracks which starts and ends when the elephant moves and stops for longer food breaks. There are also a few cases in the figures where there occur parallel tracks under short periods, this occurs when two confirmed tracks are alive at the same time. The gating threshold has been tested out with different gating probabilities and in Table 6.2 each gating thresholds gating probability are shown.

Table 6.1: *Gating thresholds and their gating probability.*

Gating threshold	Gating probability
2.70	90 %
1.64	80 %
1.07	70 %

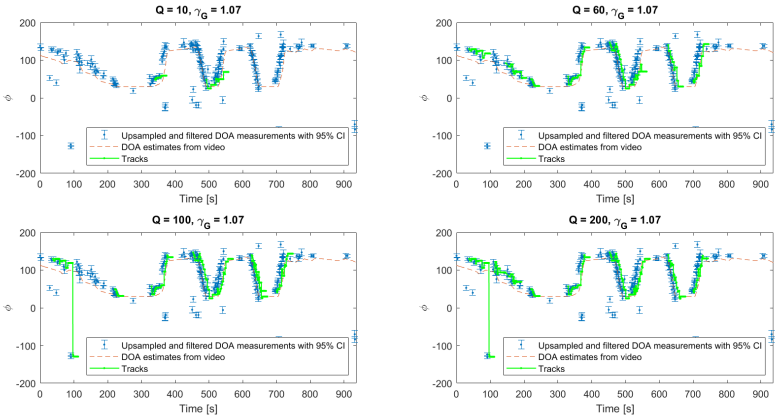

Figure 6.1: *DOA tracking of elephant footsteps with a CP motion model and gating threshold* $\gamma_G = 1.07$.

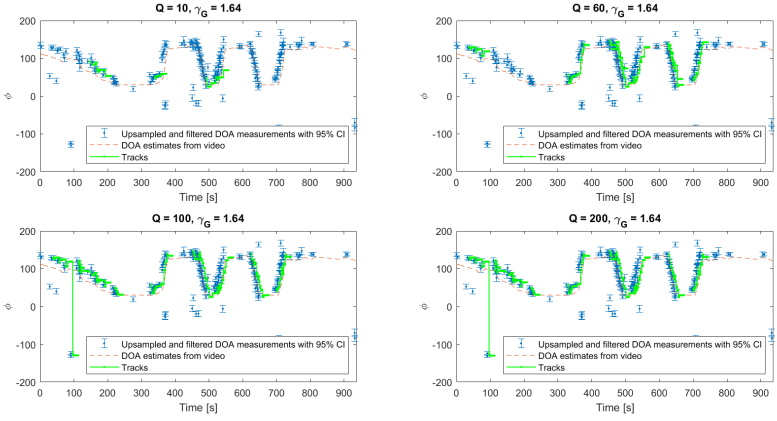

Figure 6.2: *DOA tracking of elephant footsteps with a CP motion model and gating threshold* $\gamma_G = 1.64$.

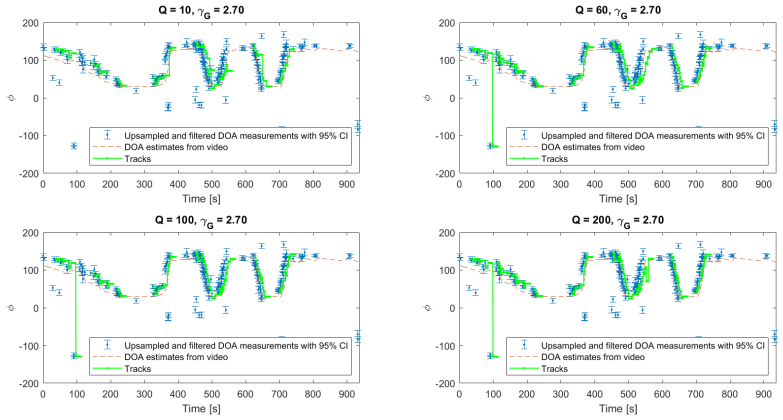

Figure 6.3: *DOA tracking of elephant footsteps with a CP motion model and gating threshold* $\gamma_G = 2.70$.

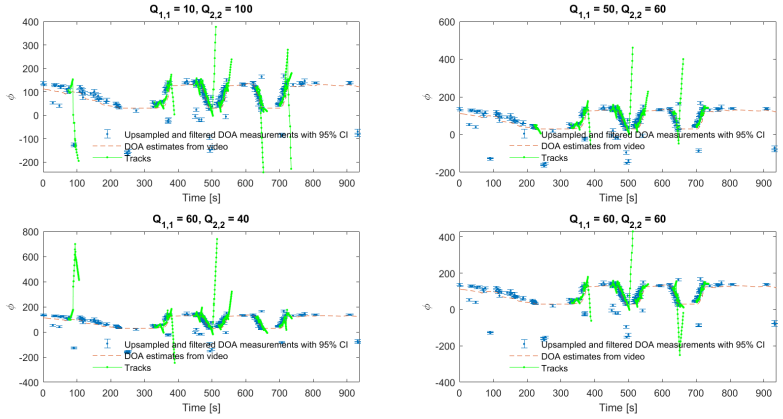

Figure 6.4: *DOA tracking of elephant footsteps with a CV motion model*

Multiple target

During the data collection at Kolmården, data was also collected for a smaller elephant herd (3 elephants). For the tracking, the elephants could not be separated as individual tracks, since they were very close to each other all the time. Therefore, was another dataset collected at Vallamassivet where two humans walked at the same time from different directions. This dataset is used to evaluate how the DOA measurements are affected when multiple seismic waves interfere and to investigate if the described tracking system in Section 6.3 can identify multiple targets. In Figure 6.5 the results for this is shown with a KF with an CP motion model with the gating threshold $\gamma_G = 1.07$ and model noise $Q = 80$.

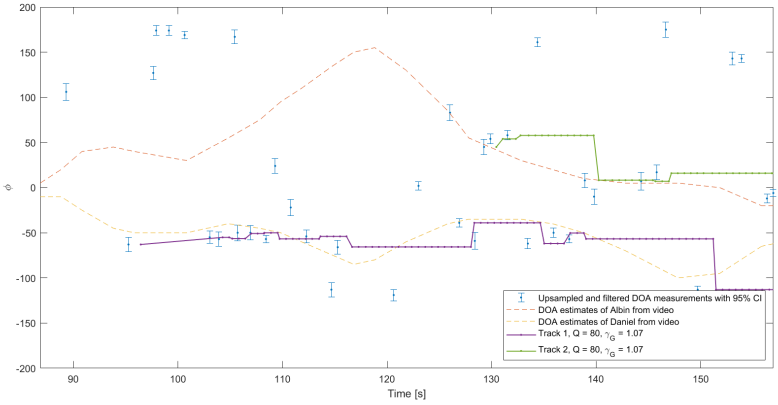

Figure 6.5: *DOA measurements for two walking humans.*

6.4.2 Position tracking

Separate DOA measurements

In Figure 6.6 the created position tracks for separate DOA measurements are shown with different design.

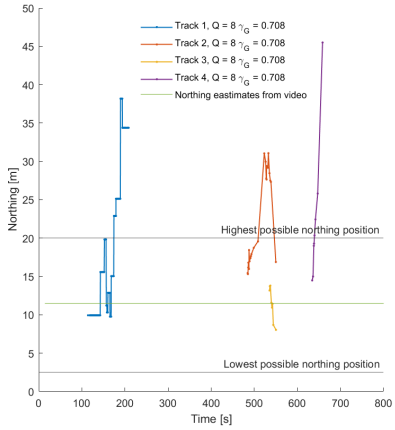

(a) *Northing estimates from a EKF based on separate DOA measurements with model noise of $Q = 8$ and gating threshold $\gamma_G = 0.708$.*

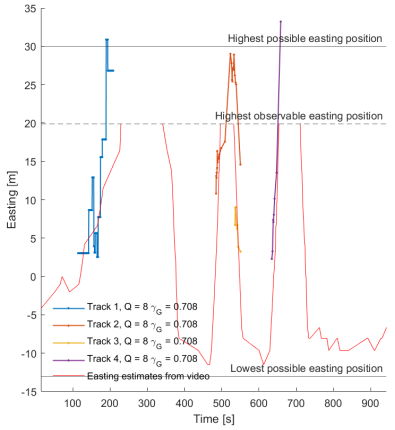

(b) *Easting estimates from a EKF based on separate DOA measurements with model noise of $Q = 8$ and gating threshold $\gamma_G = 0.708$.*

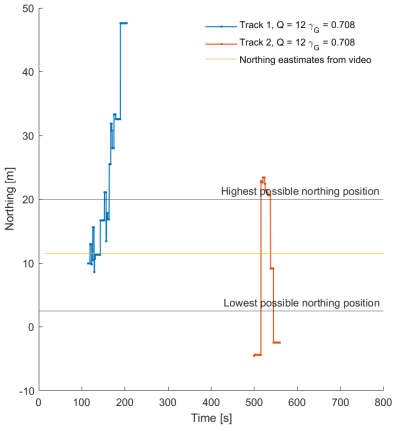

(c) *Northing estimates from a EKF based on separate DOA measurements with model noise of $Q = 12$ and gating threshold $\gamma_G = 0.708$.*

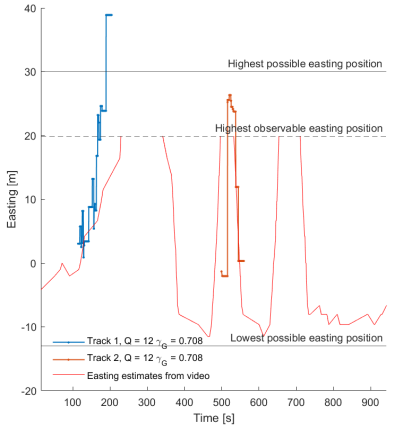

(d) *Easting estimates from a EKF based on separate DOA measurements with model noise of $Q = 12$ and gating threshold $\gamma_G = 0.708$.*

Figure 6.6

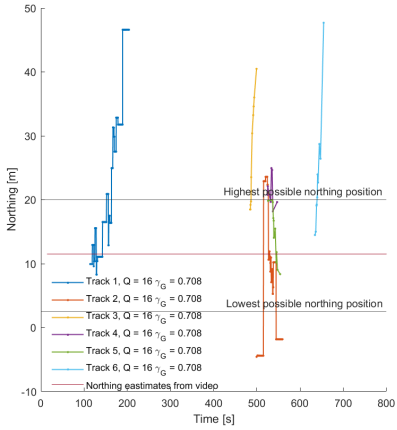

(e) *Northing estimates from a EKF based on separate DOA measurements with model noise of $Q = 16$ and gating threshold $\gamma_G = 0.708$.*

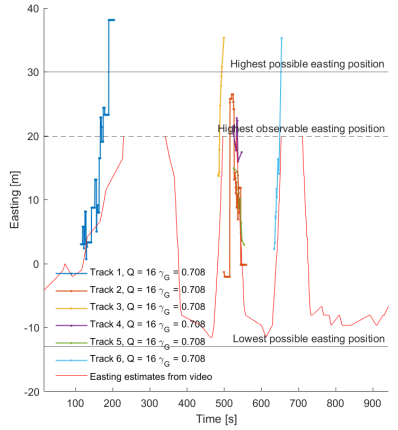

(f) *Easting estimates from a EKF based on separate DOA measurements with model noise of $Q = 16$ and gating threshold $\gamma_G = 0.708$.*

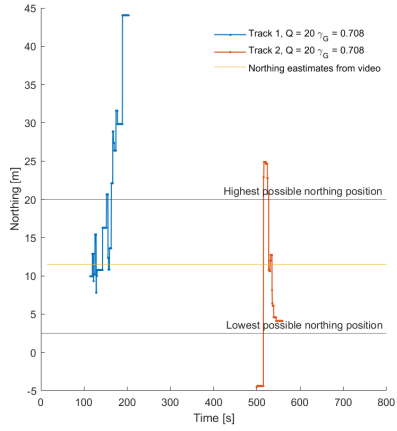

(g) *Northing estimates from a EKF based on separate DOA measurements with model noise of $Q = 20$ and gating threshold $\gamma_G = 0.708$.*

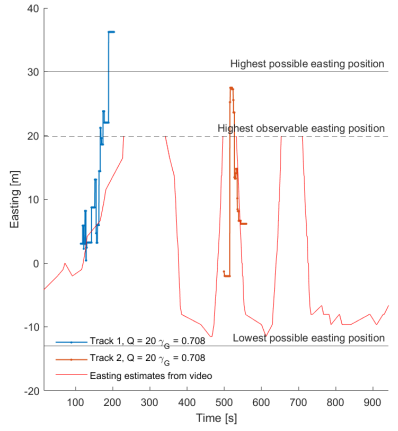

(h) *Easting estimates from a EKF based on separate DOA measurements with model noise of $Q = 20$ and gating threshold $\gamma_G = 0.708$.*

Figure 6.6: *Localisation estimates of an elephant using an EKF based on separate DOA measurements with a CP motion model.*

Triangulated DOA measurements

This filter used the triangulated DOA measurements from Section 5.9.6 as measurements. The measurement noise was chosen as

$$R = \begin{pmatrix} 100 & 0 \\ 0 & 100 \end{pmatrix}$$

since the measurements from Section 5.9.6 had variance of 100 while in reality they should have had a variance of maximum 25. The filter was then tuned to adapt to changes in the measurements in a reasonable speed by changing the model noise Q while applying gating as well. The gating threshold has been tested out with different gating probabilities and in Table 6.2 each gating thresholds gating probability are shown.

Table 6.2: *Gating thresholds and their gating probability.*

Gating threshold	Gating probability
1.3467	49 %
1.3863	50 %
4.2405	88 %
4.4145	89 %
∞	100 %

In Figure 6.7 and Figure 6.8 are some of tested filter in the tuning phase shown. The measurements were divided into four parts, since there were parts where the elephant didn't move. In Figure 6.7 is the yellow line KF measurement updates, the red dashed line are estimates from the video and the blue dots are measurements. In Figure 6.8 is the yellow line KF measurement updates and the green dots are the measurements.

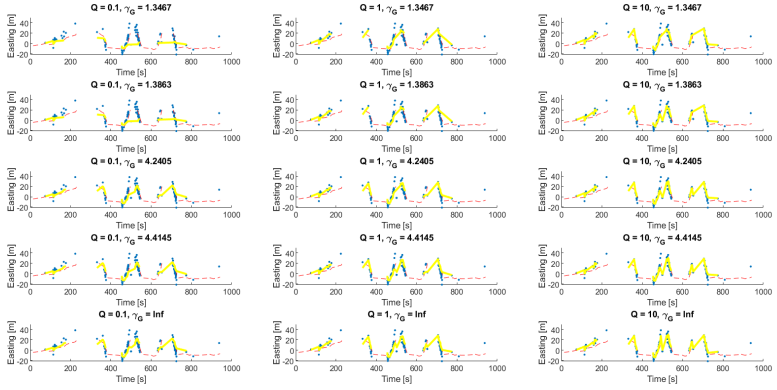

Figure 6.7: *Easting estimates from a Kalman filter based on triangulated DOA measurements.*

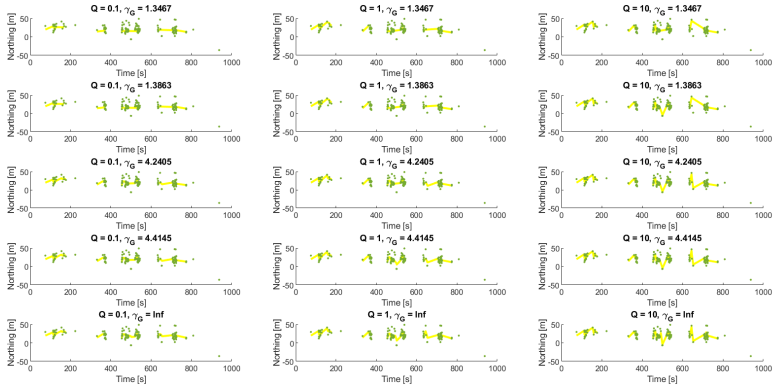

Figure 6.8: *Northing estimates from a Kalman filter based on triangulated DOA measurements.*

In Figure 6.9 and Figure 6.10 are the best designed filter results shown.

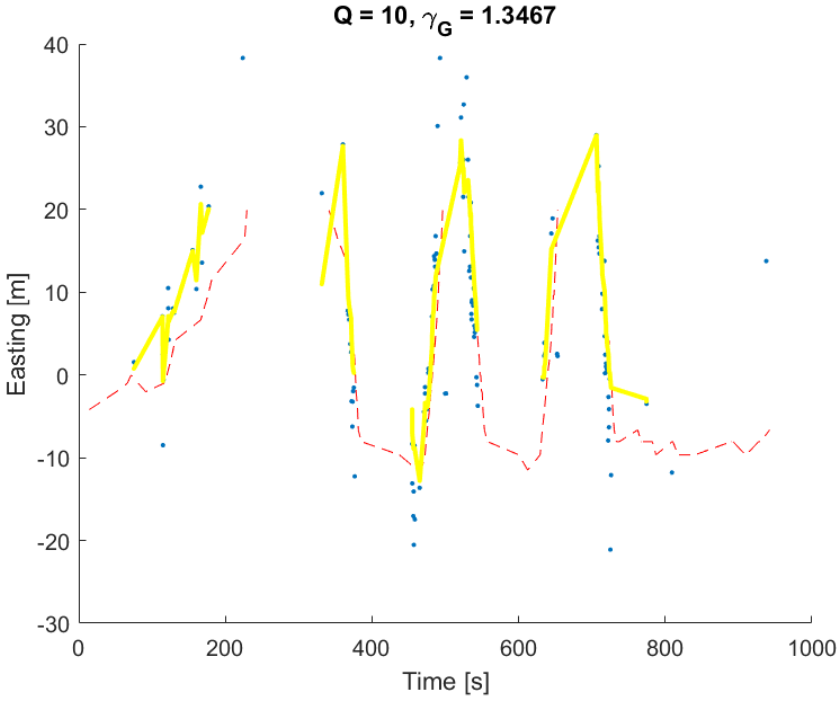

Figure 6.9: *The best designed KF, based on triangulated DOA measurements, easting estimates.*

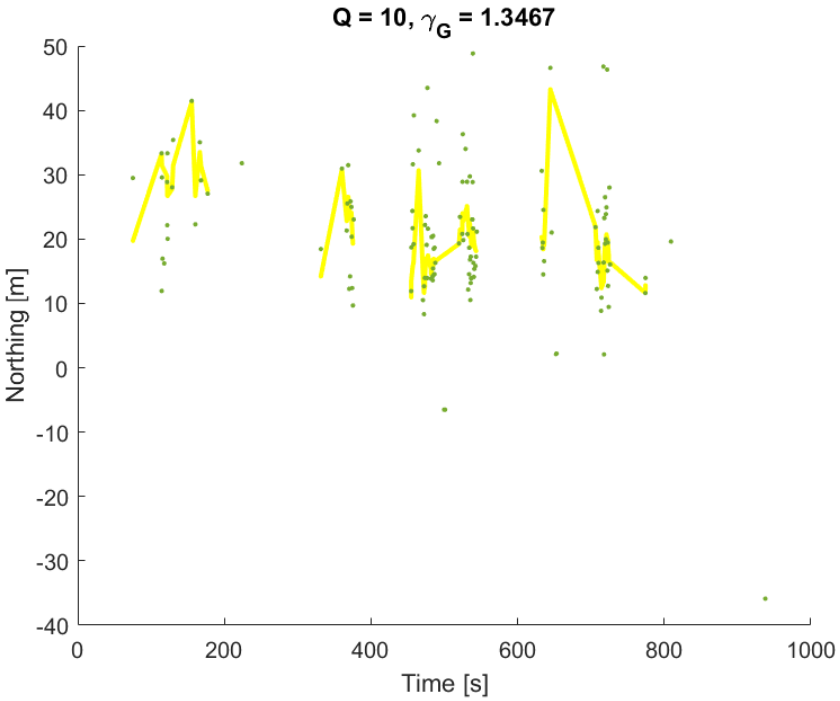

Figure 6.10: *The best designed KF, based on triangulated DOA measurements, northing estimates.*

In Figure 6.11 are the four created tracks shown for the best designed filter.

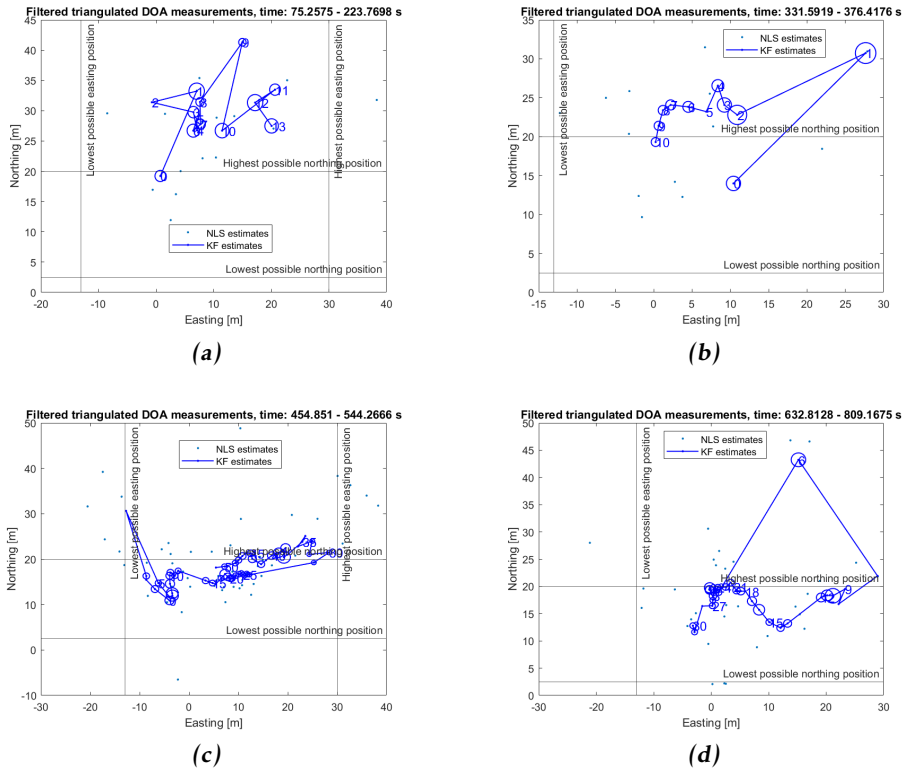

Figure 6.11: *Measurement updates from the best designed KF based on triangulated DOA measurements.*

6.5 Discussion

This section discusses the result of both the DOA tracking filter and the position tracking.

6.5.1 DOA tracking

This section discusses the result of the DOA tracking filter.

Single target

In Figure 6.1, Figure 6.2 and Figure 6.3 the created tracks for the DOA tracking with a CP motion model are presented. From the figures it can be seen that with higher model noise more measurements gets associated with the track as expected and the same follows for higher gating threshold. But with too high gating threshold and model noise, the risk of accepting false measurement increases. In the presented tracks this is no major problem, all tracks seem to have

updates which are near to the estimates from the video where the amount of outlier increases mainly by the gating threshold which can be seen for $Q = 60$ where outliers are present first with a gating threshold of $\gamma_G = 2.70$, although all the tracks with outliers have similar amount of outliers. With higher model noises and low gating threshold, outliers will be present also, which can be seen in Figure 6.1. There are also some cases where multiple tracks are confirmed, alive and identified as separate targets at the same time, as when $Q = 60$ and $\gamma_G = 1.64$ or when $Q = 100$ and $\gamma_G = 1.07$. For both of these cases, the gating threshold is quite low and this means that a measurement has a smaller probability of being accepted to these tracks. Thereby does the risk of multiple tracks increase when tracks accept fewer measurements.
It may also seem like the filter is quite slow to adapt to changes in the measurements, even when the model noise is high. Since the filter is based on a multi target tracking system there will be multiple existing tracks, while most of them are going to be tentative and not visible in the results. Although do these tentative tracks require computational resources as well, for example for time updating. This means that there may be a smaller delay between when a detection occur and when a measurement update happens, depending on the number of tracks.

In Figure 6.4 the created tracks for the DOA tracking with a CV motion model are presented. The filter estimates the velocity quite poorly and when the tracks get no measurements, the DOA is predicted most often with a high velocity and the DOA predictions gets quickly bad for most of the filters and their tracks with some exceptions as when $Q_{1,1} = 60$ and $Q_{2,2} = 60$ and when $Q_{1,1} = 50$ and $Q_{2,2} = 60$ where the last track of the filters predicts the DOA to be almost constant. One problem for the velocity estimation is that the filter needs to get at least two measurement from the same direction to estimate the velocity close to 0 but most often did the elephant stop directly without a noticeable retardation.

To choose the best design for the filter, one must consider the pros and cons of each design parameter. By having a low gating threshold, fewer measurements will be associated with the track and the probability of associating false measurements will decrease. Meanwhile, the gating threshold can not be too low to get measurements in the first place. From the results, $\gamma_G = 1.64$ can be considered as a good gating threshold, since the filters with model noise of $Q = 100$ and $Q = 200$ performs similar to the filter with equal model noise but higher gating threshold.

Bigger model noises will make the track uncertain quicker, and the risk of accepting false measurements will increase by that. Therefore, the model noise should not be too big. By these arguments and the presented results, the best and most suitable design parameter for tracking an elephant with CP motion model is $Q = 100$ and $\gamma_G = 1.64$ in Figure 6.2. These parameters had a pretty big outlier in the beginning, which is because a higher Q, which leads to the filter listening more to the measurements. Other than this outlier, the tracking looks very good and because of this it can still be regarded as a good choice of design parameters.

Multiple target

In Figure 6.5, a KF with a CP motion model and model noise of $Q = 80$ and gating threshold of $\gamma_G = 1.07$ is used. Many other designs of this filter have been tested, and the presented filter gave the best result for this dataset, based on two walking humans. Firstly, by comparing the DOA measurements with the estimates from the validation, it is not super clear that there are measurements which belong to either Albin or Daniel. The filter gives out two tracks, one track exist during almost the whole dataset and is similar to Daniel's path. The other track is much shorter but is similar to Albins path. The result is not great, but one error could be that the data was collected only using kurtosis detection and no other signal features. This results in worse segments for the DOA estimates. Considering this, one can still see that the created pattern can be associated with two walking humans and even with quite good performance for Daniel. Another reason of the poor DOA measurements could be the that the footsteps from Albin and Daniel does interfere with each other and therefore, some of the DOA measurements could be quite confusing for the algorithm. To be able to draw a conclusion, longer datasets are needed and also data of separable elephant herds are needed for maximising our system with both the designed detection algorithm, which has shown to give good DOA measurements, and for the track logic which is designed from detections and observations of elephants.

6.5.2 Position tracking

Separate DOA measurements

In Figure 6.6, the created position tracks using separate DOA measurements are presented. The initial value of the tracks are good since, they are triangulated. The update seems quite strange though. Both the updates in the easting and northing positions behave in the similar patterns. Why the filter behave like this could be because of poor design of the filter, implementation error or as simple as the model does not suit the filter or vice versa. Another reason for the poor updates can be that the track gets more measurement from one device, resulting in that the track only being able to update the position accurately in one direction, and poorly in the other. The EKF struggles with the northing position, just as the localisation did. It is unclear if it could be for the same reasons or not. The easting tracks, however, show some more promising results. All designs somehow follow the easting position. In Figure 6.6f, there are quite a lot of tracks, making $Q = 16$ a bad candidate. Figure 6.6b, Figure 6.6d and Figure 6.6h all have a more reasonable amount of track, but $Q = 8$ is the only one of the three that creates a track when the elephant walks back and forth a third time. Out of all the filters, this one seams the most feasible.

Triangulated DOA measurements

In Figure 6.11 are the best designed position tracks shown. The tracking in the eastern axis shows promising results, and it is clear that the elephant walks back and forth in the eastern axis. In Figure 6.11c and Figure 6.11d does the filter give overall good localisation estimates, where even the northern position isn't too big with a few exceptions and the majority of the estimates are inside the fence. The few outliers in the northing position are also in the beginning of the track, see Figure 6.10, if the initial state covariance is decreased these outliers may disappear. As the filter gets more measurements, the number of outliers are drastically decreasing, this shows that the filter is good tuned for tracking elephants. The filter seems to handle the discussed bias in the northern position quite well in most of the cases, and if the northing position is better estimated, this filter would a good option for tracking elephants.

7

Conclusion

In this thesis, a system for detecting elephant footsteps have been developed. Software has been written that can somewhat estimate and track the position of the elephant when multiple devices are used. In the case of one device, the direction of the elephant can be estimated and tracked.

Two elephant detection algorithms have been tested. In the end, the signal feature method was the most appropriate for the device. It can detect elephant footsteps with an accuracy of 89 % and detects 54 % of elephant footsteps. It is able to differentiate elephants from other animals quite well, and has low false alarm rate.

An elephant's direction relative to one geophone array can be estimated fairly good. A big majority of the estimates are really close to the elephant and by applying a Kalman filter with a CP motion model an elephant can be tracked as an individual with estimates which consist of almost no outliers. Results have also shown that the filter for the elephant tracking can distinguish multiple humans as separable targets to some extent.

The localisation worked quite well in the eastern direction, but did not manage to give good results in the northern direction. This could be due to many different sources of error. The tested EKF did not perform good enough to be used for tracking of an elephant's localisation with the current design and implementation. Like the localisation, it showed some promise in the easting tracking but in the northing direction, it had some strange behaviour. This could be caused by bad implementation, bad tuning or a bad choice of filter for the application. The tested KF based on triangulated DOA measurements performed well and could track the elephant in most of the cases with high enough performance and especially when there weren't too many high northing measurements.

7.1 Further work

There are a lot of things that could be done in the future to improve upon this work. One thing is to work on improving the detection algorithm further. One could look at more signal features to improve accuracy, or turn to machine learning for detections. This would however need a lot of data, which isn't available right now. If machine learning is used, one could develop a sensor that does not only detect elephants, but detects and classifies all kinds of animals. This would make the device even more versatile.

Another subject that could be investigated in the future, is to count detected individuals in a herd. Counting animals is an important part of a park ranger's work, and if this could be automated, it would help them a lot. This could possibly be done by a combination of methods, like the tracking with gating used in this thesis, energy registered by the geophone, and by looking at gait and how many footsteps that are registered each second.

The tracking of the elephant localisation from this report has been shown varying results. For the implemented EKF, based on separate measurements, does this depend on the filter updates mainly. To improve the tracking of the localisation, the described filter could be either further developed or investigated.

The localisation estimates have also shown to have a bias in the northing position and a bigger variance than expected. If the cause of this problem is solved, the KF based on triangulated DOA measurements can be further developed and the covariance from the localisation estimates could be used to model the measurement noise in the filter, to improve the filter performance.

If the localisation is improved upon, the position of the elephant could be used to make a model for how the energy of a footstep decreases with distance. With this model, it would be possible to estimate the weight of an elephant when a detection is made.

Bibliography

[1] Elephants their families: The importance of social structures within a herd, . URL https://herd.org.za/blog/elephants-their-families-the-importance-of-social-structures-within-a-herd/.

[2] The unique sleeping habits of african elephants, . URL https://www.safariventures.com/the-unique-sleeping-habits-of-african-elephants/.

[3] Petre Anghelescu, Gabriel Vasile Iana, and Ionut Tramandan. Human footstep detection using seismic sensors. In *2015 7th International Conference on Electronics, Computers and Artificial Intelligence (ECAI)*, pages AE–1–AE–2, 2015. doi: 10.1109/ECAI.2015.7301179.

[4] George Athanasopoulos, Panagiotis Pelekis, and G.A Anagnostopoulos. Effect of soil stiffness in the attenuation of rayleigh-wave motions from field measurements. *Soil Dynamics and Earthquake Engineering*, 19:277–288, 06 2000. doi: 10.1016/S0267-7261(00)00009-9.

[5] Carl de Boor. *A Practical Guide to Splines*. Springer-Verlag, 1978.

[6] Dimensions. African bush elephant (loxodonta africana). URL https://www.dimensions.com/element/african-bush-elephant-loxodonta-africana.

[7] Ettagbor Hans Enukwa. Human-elephant conflict mitigation methods: A review of effectiveness and sustainability. *Journal of Wildlife and Biodiversity*, 1(2):69–78, Oct. 2017.

[8] *ESP32 Series Datasheet*. Espressif Systems, 2023. Version 4.2.

[9] Mille Millnert Fredrik Gustafsson, Lennart Ljung. *Signal Processing*. Studentlitteratur, third edition, 2011.

[10] Olivia Garcia. How do elephants get their food? URL https://elephantguide.com/en/how-do-elephants-get-their-food/.

[11] Rickard Karlsson Gustaf Hendeby. Single target tracking, 2022. URL https://mtt.edu.hendeby.se/file/le3.pdf.

[12] Fredrik Gustafsson. *Statistical Sensor Fusion*. Studentlitteratur, third edition, 2018.

[13] Fredrik Gustafsson. Scale and delay estimation. 2021.

[14] Gökhan Koç and Korkut Yegin. Footstep and vehicle detection using slow and quick adaptive thresholds algorithm. *International Journal of Distributed Sensor Networks*, 9(10):783604, 2013.

[15] Joos Korstanje. The f1 score. URL https://towardsdatascience.com/the-f1-score-bec2bbc38aa6.

[16] Unjung Nam. Special area exam part, 2001. URL https://ccrma.stanford.edu/~unjung/AIR/areaExam.pdf.

[17] R Nave. Seismic waves. URL http://hyperphysics.phyastr.gsu.edu/hbase/Waves/seismic.html.

[18] C. E. O'Connell-Rodwell, B. T. Arnason, and L. A. Hart. Seismic properties of Asian elephant (Elephas maximus) vocalizations and locomotion. *The Journal of the Acoustical Society of America*, 108(6):3066–3072, 12 2000.

[19] CE O'Connell-Rodwell, BT Arnason, and LA Hart. Seismic properties of asian elephant (elephas maximus) vocalizations and locomotion. *The Journal of the Acoustical Society of America*, 108(6):3066–3072, 2000.

[20] Shijia Pan, Ningning Wang, Yuqiu Qian, Irem Velibeyoglu, Hae Young Noh, and Pei Zhang. Indoor person identification through footstep induced structural vibration. In *Proceedings of the 16th International Workshop on Mobile Computing Systems and Applications*, HotMobile '15, page 81–86, New York, NY, USA, 2015. Association for Computing Machinery.

[21] Rohit Samkaria, Rajesh Singh, Anita Gehlot, Rupendra Pachauri, Amardeep Kumar, Neeraj Kumar Singh, and Kaushal Rawat. IOT and XBee triggered based adaptive intrusion detection using geophone and quick response by uav. *International Journal of Engineering & Technology*, 7(2.6):12–18, 2018.

[22] *SM-24 Geophone Element*. SENSOR Nederland b.v, 2006.

[23] L. Jen Shaffer, Kapil K. Khadka, Jamon Van Den Hoek, and Kusum J. Naithani. Human-elephant conflict: A review of current management strategies and future directions. *Frontiers in Ecology and Evolution*, 6, 2019.

[24] Philip Sjövik and Erik Wahledow. Detection and localization of elephants using a geophone network. Master's thesis, Linköpings universitet, 2022. URL http://urn.kb.se/resolve?urn=urn:nbn:se:liu:diva-193109.

[25] PJ Stephenson. *The future for elephants in Africa.*, pages 133–136. 01 2004.

[26] *Very Low Noise, 24-Bit Analog-to-Digital Converter*. Texas Instruments, 6 2003. revised 2013.

[27] Khemapat Tontiwattanakul, Worathep Kusamankiat, and Somchai Jaksan. Design and signal processing for acoustic compass. pages 117–120, 2021. doi: 10.1109/ICEAST52143.2021.9426267.

[28] Random Nerd Tutorials. Getting started with lilygo t-sim7000g esp32 (lte, gprs, and gps). URL `https://randomnerdtutorials.com/lilygo-t-sim7000g-esp32-lte-gprs-gps/`.

[29] Jason D. Wood, Caitlin E. O'Connel-Rodwell, and Simon L. Klemperer. Methodological insights: Using seismic sensors to detect elephants and other large mammals: a potential census technique. *Journal of Applied Ecology*, 42(3):587–594, 2005.